NASA Contractor Report 156865

A Study of GEOS-3 Terrain Data with Emphasis on Radar Cross Section

R. W. Priester

May 1980

NASA

National Aeronautics and Space Administration

Wallops Flight Center
Wallops Island, Virginia 23337
AC 804 824-3411

NASA Contractor Report 156865

A Study of GEOS-3 Terrain Data with Emphasis on Radar Cross Section

R. W. Priester

Applied Science Associates, Inc.
105 East Chatham Street
Apex, North Carolina 27502

Prepared Under Contract No. NAS6-2810

National Aeronautics and
Space Administration

Wallops Flight Center
Wallops Island, Virginia 23337
AC 804 824-3411

TABLE OF CONTENTS

A STUDY OF GEOS-3 TERRAIN DATA WITH EMPHASIS ON RADAR CROSS SECTION

1.0 INTRODUCTION AND SUMMARY OF RESULTS

Although the GEOS-3 radar altimeter design was based upon achieving optimum performance during over-ocean operation, this sensor has clearly demonstrated its capability to provide useful data while tracking terrain characterized by diverse features and cover (e.g. coastal plains, swamps, ice fields, etc.). In a recent report Miller [1] showed that the GEOS-3 data can be used to:

(a) profile surface topography to within 3 meters of existing maps,

(b) detect changes in surface moisture content,

(c) discover man-made alterations in topographic features such as elevation and surface texture.

The present study, results of which are presented herein, constitutes a natural sequel to Miller's efforts in the analysis of GEOS-3 overland data. In particular, the goals of this work were as follows:

(a) develop maps of radar cross section (RCS) measurements for various terrain types,

(b) catalog the RCS of various soil and surface condition categories,

(c) determine whether or not activities such as farming and timber harvesting are detectable in RCS measurements, and

(d) analyze GEOS-3 average power return waveforms for various terrain types.

An original goal, not included in the above list, was to analyze GEOS-3 data for the great plains region and attempt to detect the effects of farming and snowfall on RCS. This phase of the study was not pursued beyond the point of examining GEOS-3 data for the area in question since, because of frequent

loss-of-lock in the tracker, the RCS data were too sparse to be used in the analysis planned. With regard to data quality used to develop the results described in this report, a fundamental premise of the effort was that no questionable data would be used. Therefore, the results contained herein are believed to be based upon the best available data, and while tracking loop jitter is accentuated over terrain, the results contained in this report are not based upon any data when the tracker was known to have lost lock.

For a definition of GEOS-3 RCS one may consult the work of Brown and Curry [2]. The definitions of RCS contained in this reference were used to compile the results presented herein.

Section 2.0 is devoted to the development of RCS maps for terrain near the east coast of the United States. Only four states were considered but the results are believed to characterize terrain of similar type and which borders a large body of water.

Analysis of GEOS-3 data for purposes of attempting to determine observable effects of farming operations is the subject of section 3.0. It is found that RCS is sufficiently altered (on a seasonal basis) so as to be observable by a radar altimeter sensor.

Section 4.0 considers seasonal variation of RCS in portions of North Carolina, South Carolina, Georgia, and Florida. The results from this portion of the study are presented as plots of RCS versus month of year.

In section 5.0 RCS of various types of subjectively categorized soil and terrain are tabulated.

An analysis of average overland return waveforms is presented in section 6.0 where it is shown, under rather stringent assumptions, that surface roughness features of some types of terrain can be extracted from GEOS-3 returns even though they are saturated.

The results obtained in section 3.0 suggest that one might use altimetry RCS data to infer the percent of a given region devoted to active farming (i.e. plowing and harvesting). This could be an important measurement in future spacebourne altimeters.

Remote sensing from space using radar altimetry has proven to be very effective for oceanographic phenomena. Future altimeter applications in regard to remote terrain sensing would benefit from a sensor specifically designed to realize a high spatial resolution. In particular, a nadir-pointing radar altimeter with high spatial resolution could provide accurate measurement of terrain elevation. It should be noted that a synthetic aperture radar cannot fulfill this function since the image formation process assumes a flat or spherical earth model.

2.0 RADAR CROSS SECTION MAPS OF TERRAIN

2.1 Introduction

In this phase of the study GEOS-3 data were used to construct maps of RCS for portions of North Carolina, South Carolina, Georgia, and Florida. Other states (e.g. Louisiana or Virginia) could have been included but it is thought that their inclusion would not have provided any new phenomenological information. The states mentioned above were selected because the GEOS-3 data set for them was dense and generally of good quality. No state was mapped entirely. For example, North Carolina data was of exceptional quality throughout the coastal plains and was good into the Sandhills region. However, as GEOS-3 approached the Piedmont Plateau, data quality rapidly deteriorated, and in addition data density decreased.

2.2 Radar Cross Section Maps for NC, SC, GA, and FL

Figure 1 illustrates the RCS map for eastern North Carolina which was developed as follows. An area search was made on the GEOS data base at Wallops Flight Center for the area of interest. This computer search of the

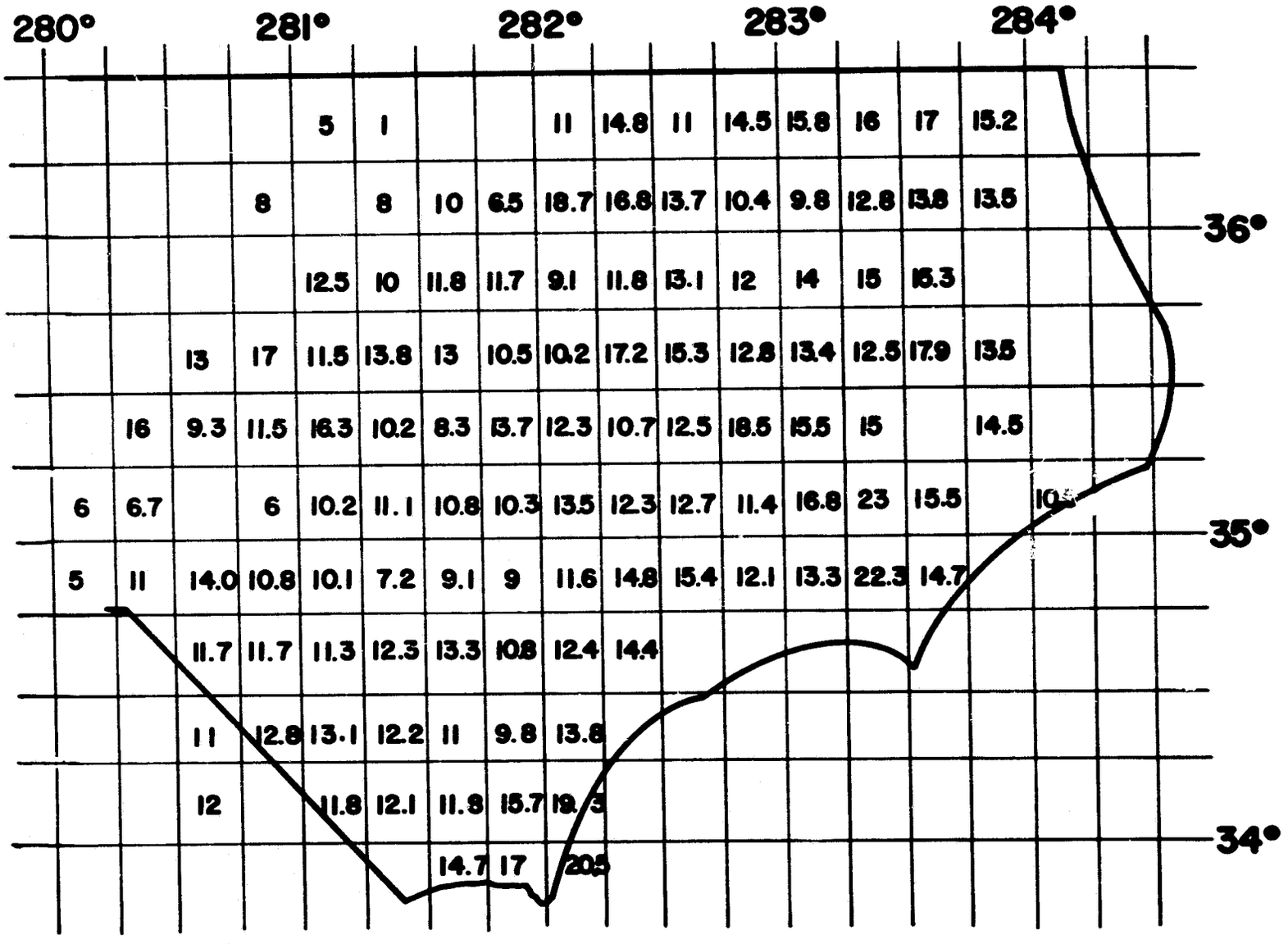

Figure 1. Radar Cross Section Map of North Carolina.

GEOS data files identified all GEOS-3 orbits which intersected the designated areas and also listed the time of entry and exit. These data from the area search were then used to obtain data of sufficient detail to allow construction of the subsatellite track on a map of the region studied. Along this ground track the frame averaged RCS values as computed at Wallops Flight Center were recorded. After all relevant data had been plotted, the map was subdivided into 0.25° squares and within each square the average RCS was computed. These resultant averages are shown within squares in Figure 1 as the RCS of the associated map area. As stated earlier, similar maps were constructed for portions of South Carolina, Georgia, and Florida and these are shown in Figures 2, 3, and 4 respectively. GEOS-3 orbits which were used in constructing these figures are tabulated in Appendix 1.

2.3 Use of the Radar Cross Section Maps

The maps developed by the above procedure are of interest for a number of reasons; these will be discussed in the remainder of this section.

2.3.1 Development of Future Overland Altimeters

Satellite altimetry offers the potential of providing accurate, complete, and detailed topographic mapping of global terrain features. These instruments do not presently exist; however, it can be stated that if maps of high quality are to be obtained from remote sensors then optimal trackers of surface features must be realized. When one considers that scattering processes encountered over terrain might consist of specular, large-body, and diffuse components (in any combination and under highly time varying circumstances) it becomes apparent that any well-designed tracker must be equipped with an adaptive mechanism which can offset such a highly dynamic environment. The data presented in Figures 1 - 4 can be of use in assessing the

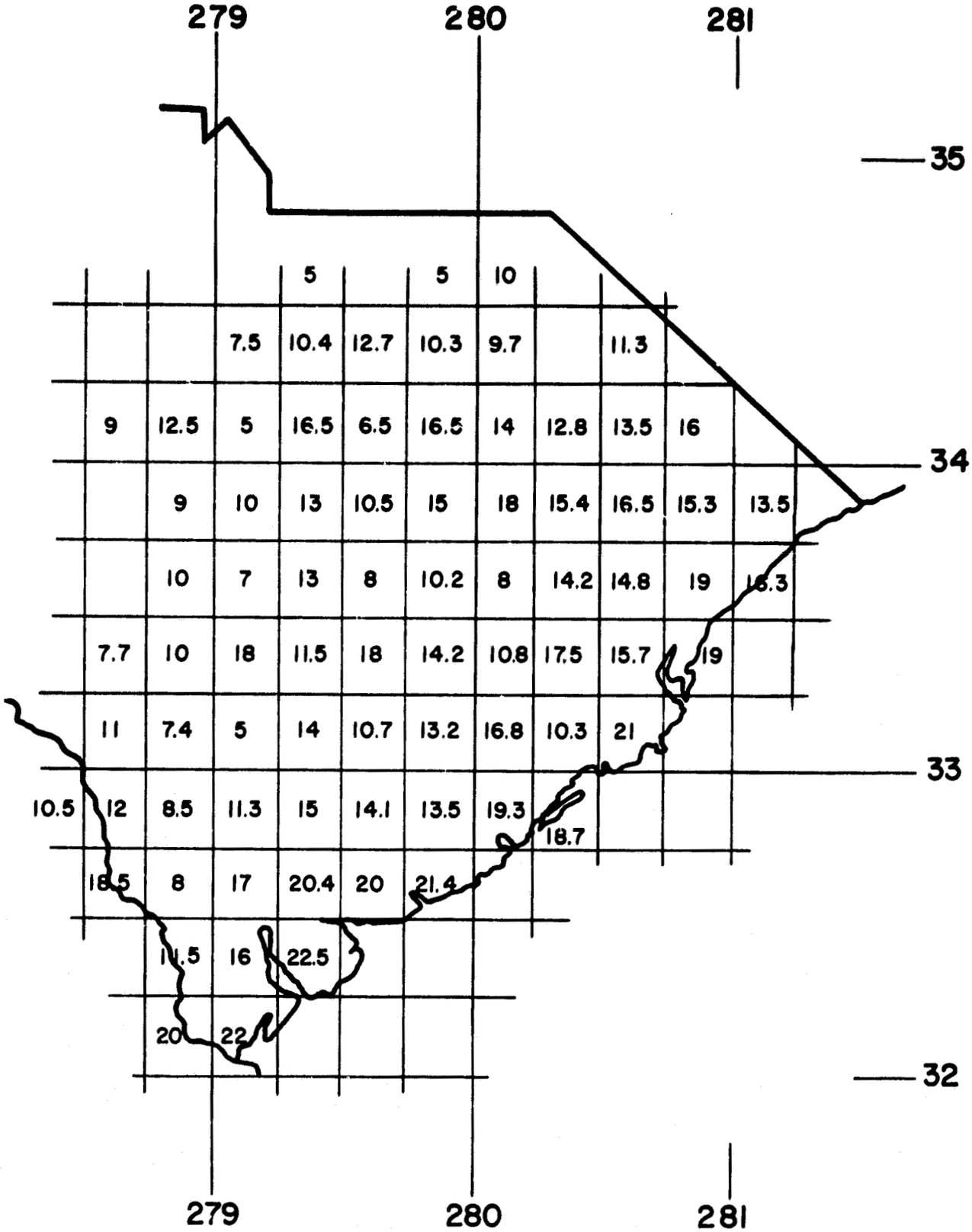

Figure 2. Radar Cross Section Map of South Carolina.

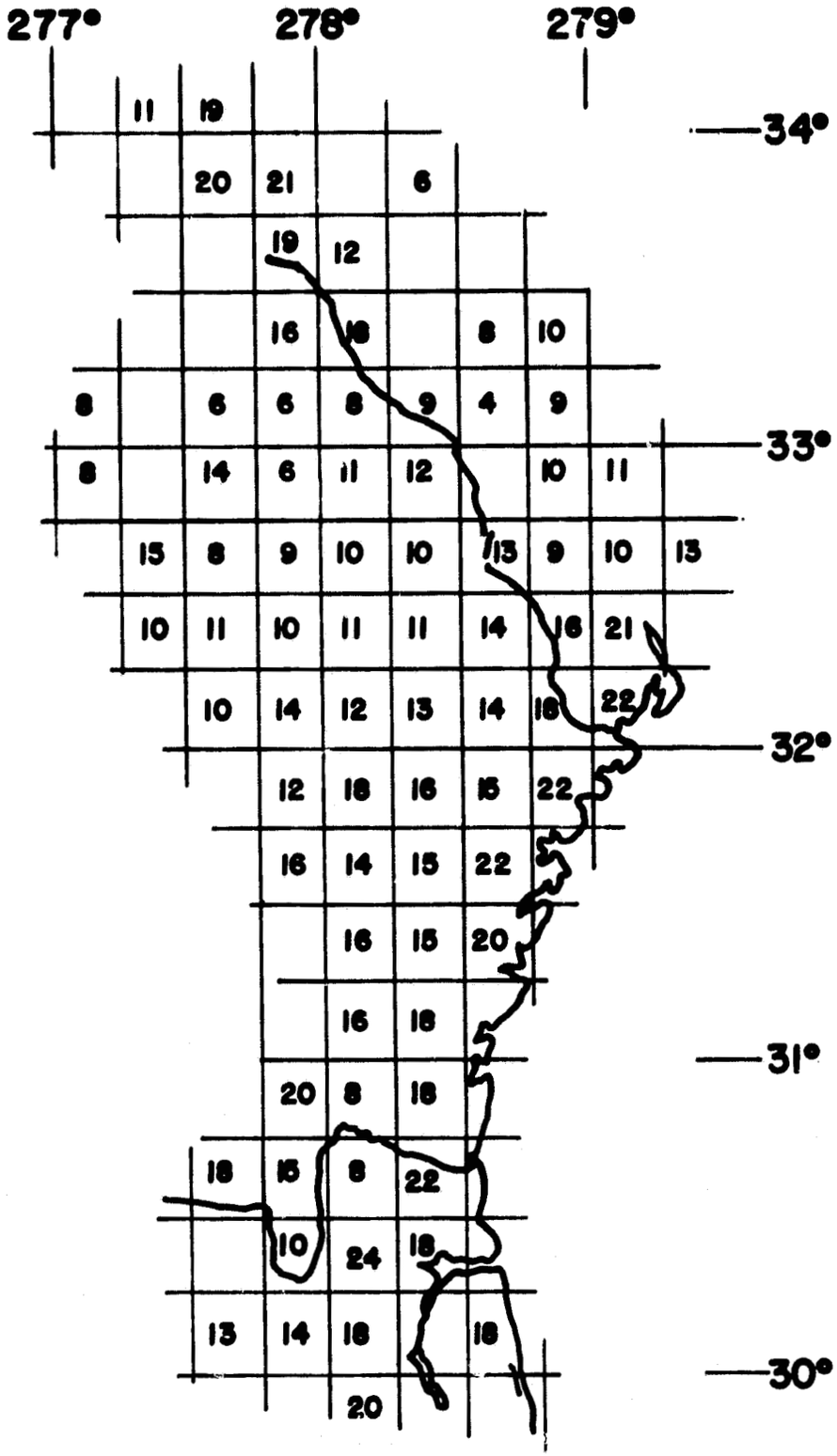

Figure 3. Radar Cross Section Map of Georgia.

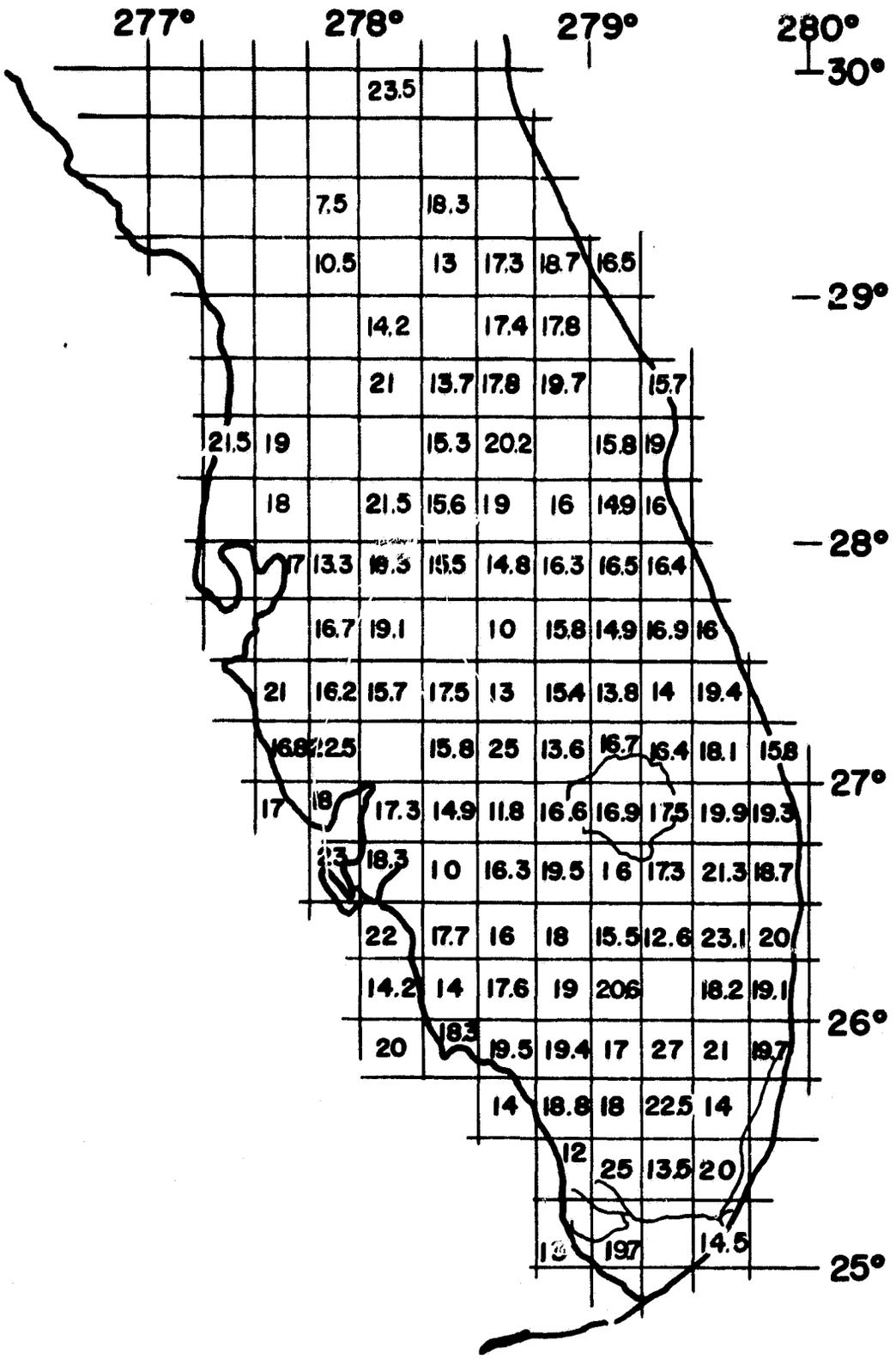

Figure 4. Radar Cross Section Map of Florida.

variability of RCS to be expected when an altimeter operates over the applicable terrain.

2.3.2 Construction of Radar Cross Section Curves Versus Inland Distance

The RCS maps presented above have been used to develop curves which describe the way in which RCS changes as one progresses inland from the land/sea interface (the inland progression is prescribed to be generally perpendicular to the land/sea interface). Curves of this type which were developed in the course of the study are applicable only to the situation where the coastal region is essentially flat (marshy and swampy) and makes a gradual transition to higher terrain which consists of gently rolling hills. Curves for North Carolina, South Carolina, Georgia, and Florida are shown in Figures 5-8 respectively. In these figures the average RCS is denoted by solid disks while the one-sigma deviations from the average are shown as vertical bars. As can readily be seen, average RCS varies approximately exponentially versus inland distance for all states studied (converging toward a constant asymptote). The geometry of the portion of Florida that was studied leads to a somewhat different presentation as shown by Figure 8. If the two branches (east and west sections of the Florida peninsula) are combined into a single plot, the result shown in Figure 9 is obtained. Figure 10 is a plot of average RCS, for each state studied, drawn on a common scale. There is consistent agreement among the curves except that the average RCS of Florida decreases less rapidly than the other regions as inland distance increases.

Maximum one-sigma deviations about the curves presented here are approximately 4 dB; however, for rougher, more inhomogeneous terrain (such as mountainous regions) much larger variation has been reported [1] (it is important to note that the one-sigma value stated here applies to the averaged data shown on the RCS maps). Therefore, it must be emphasized that the average

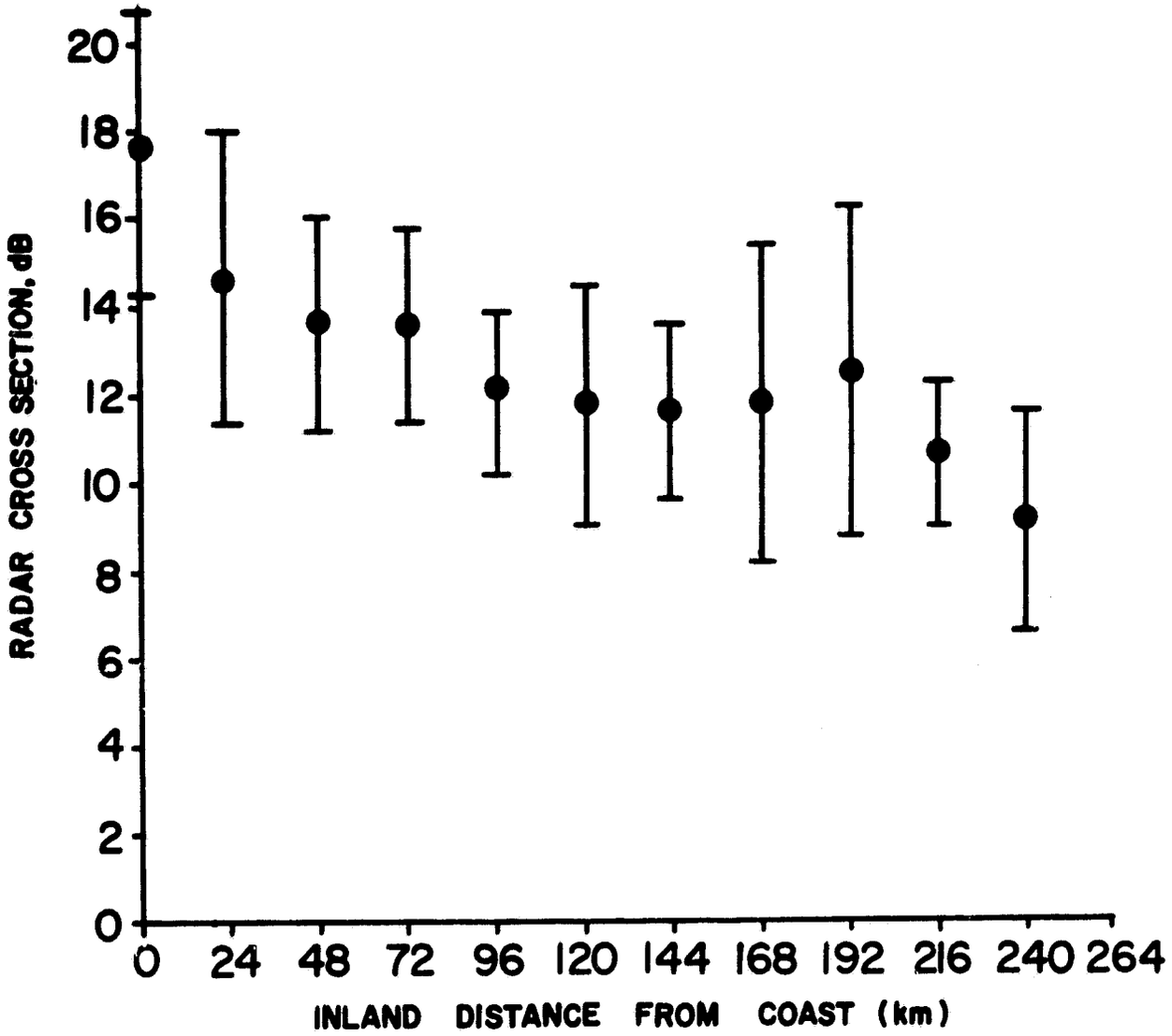

Figure 5. Variation of average Radar Cross Section versus inland distance for North Carolina.

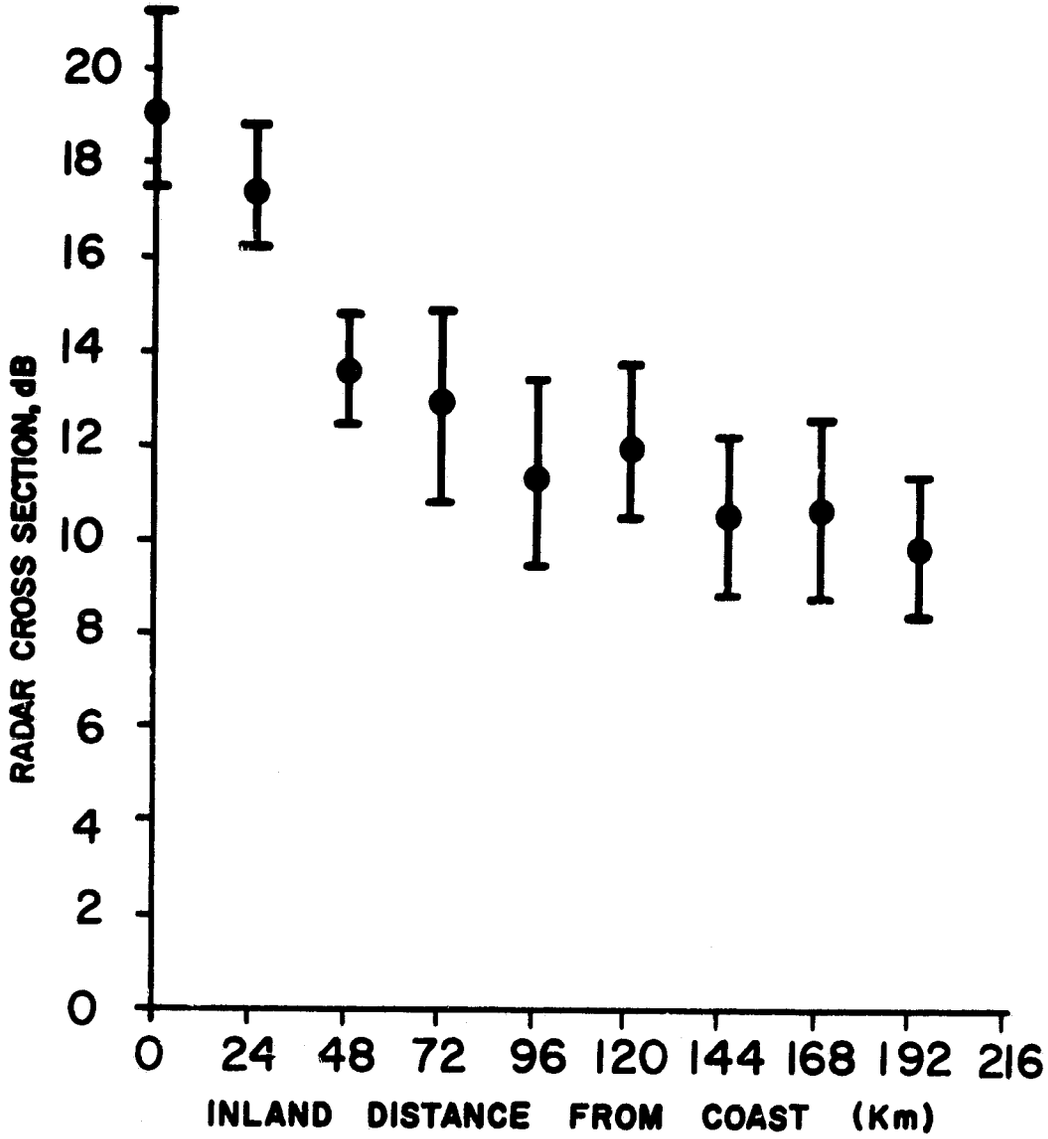

Figure 6. Variation of Radar Cross Section versus inland distance for South Carolina.

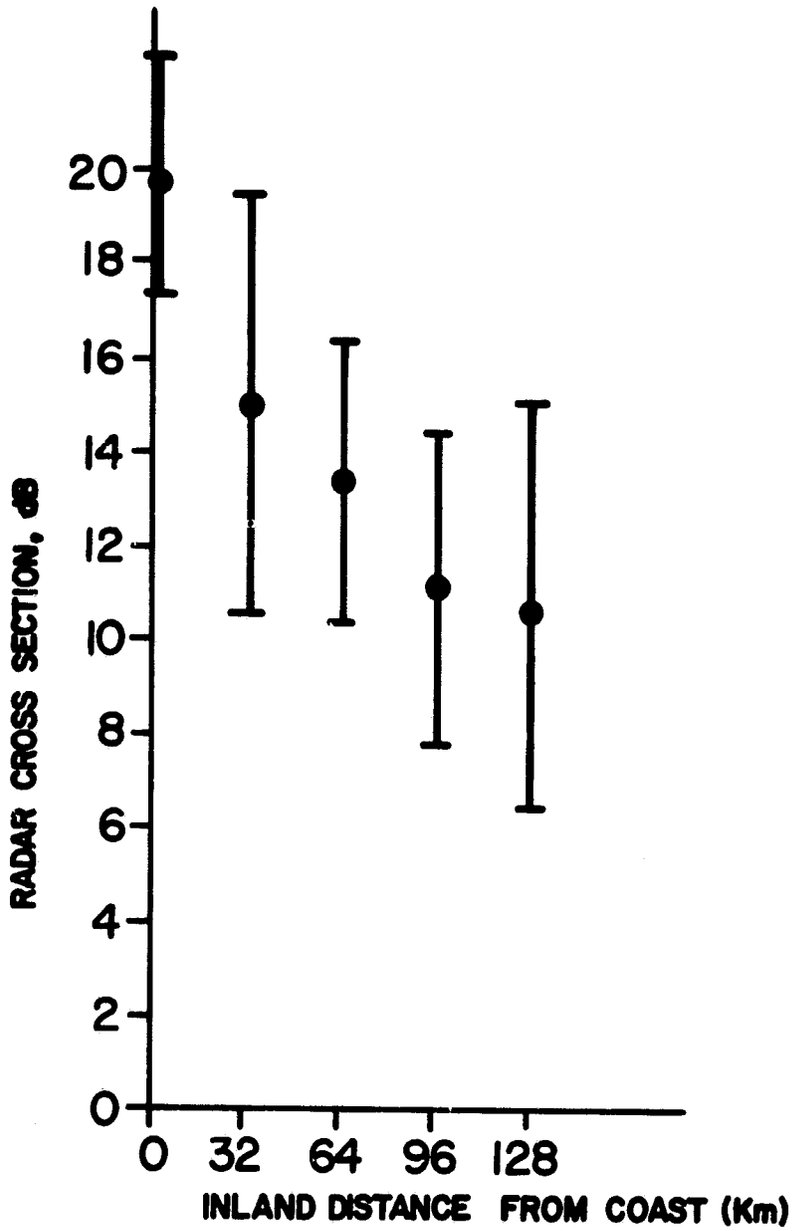

Figure 7. Variation of Radar Cross Section versus inland distance for Georgia.

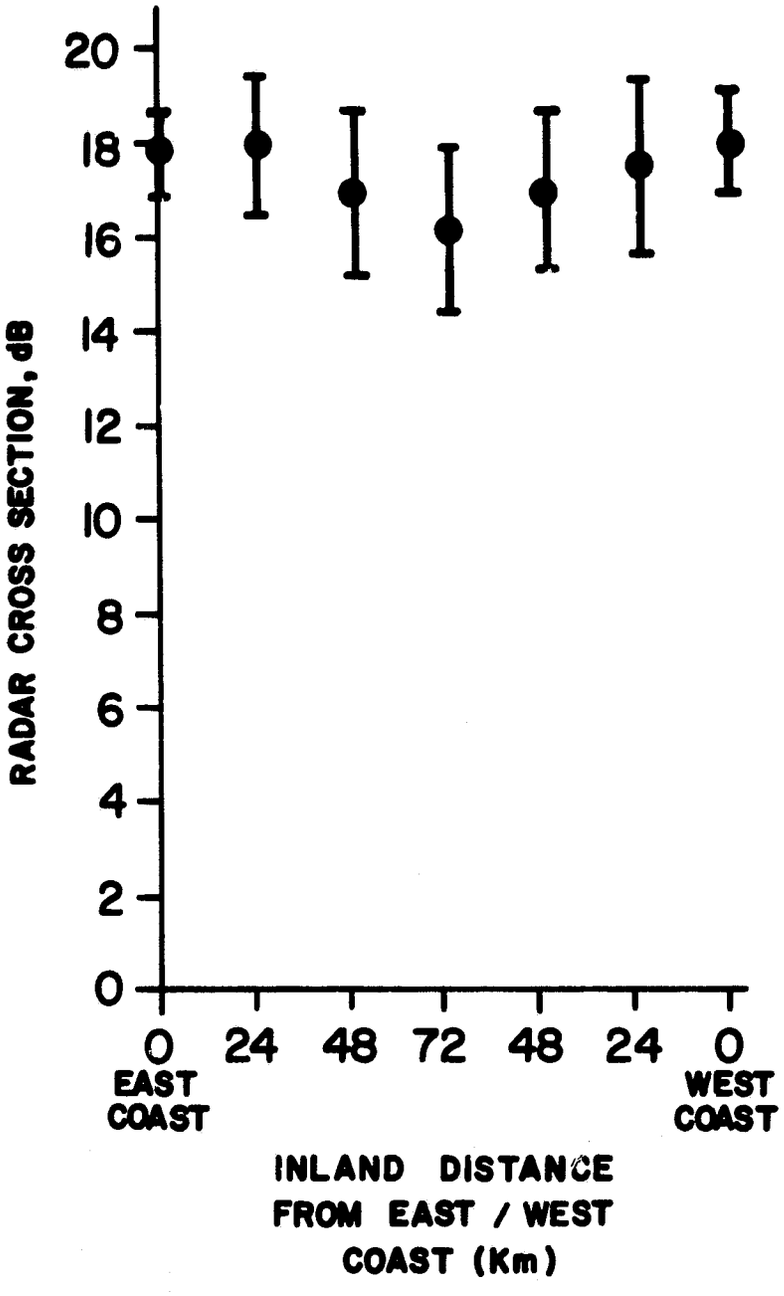

Figure 8. Variation of Radar Cross Section versus inland distance for Florida.

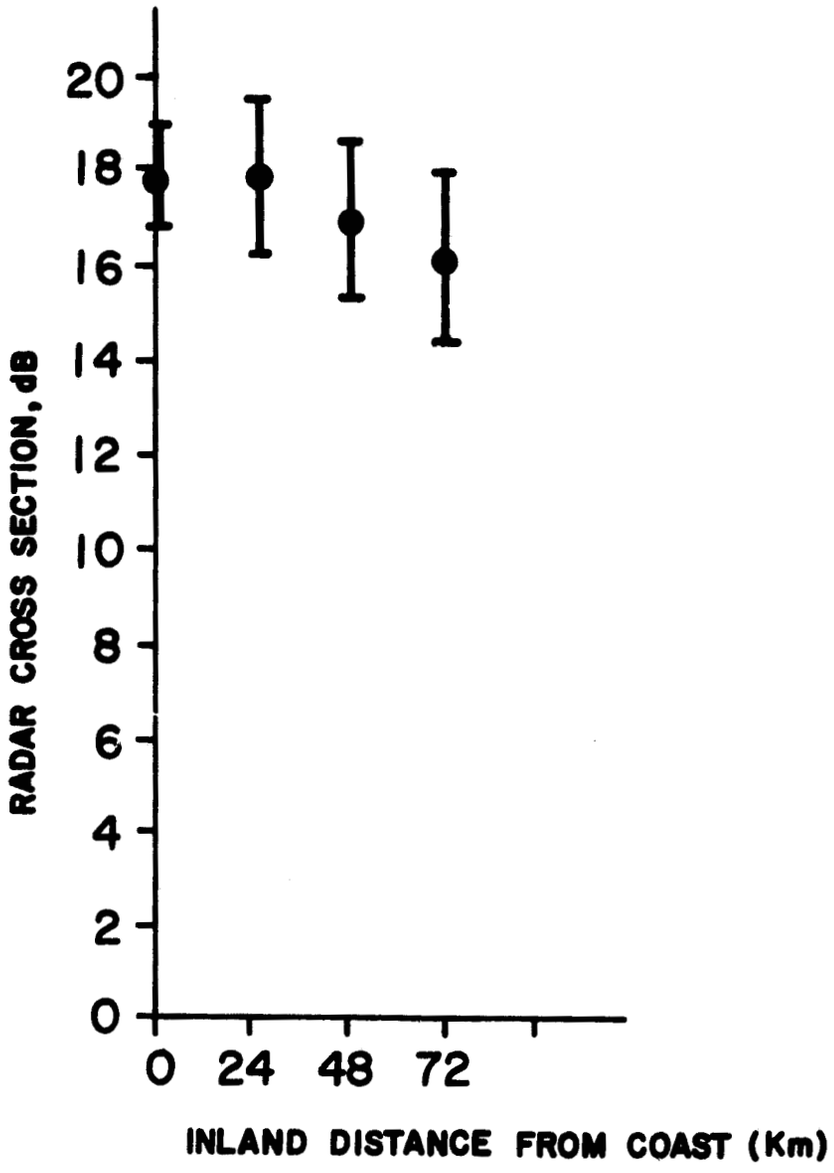

Figure 9. Variation of Radar Cross Section versus inland distance for Florida (combined east and west coasts).

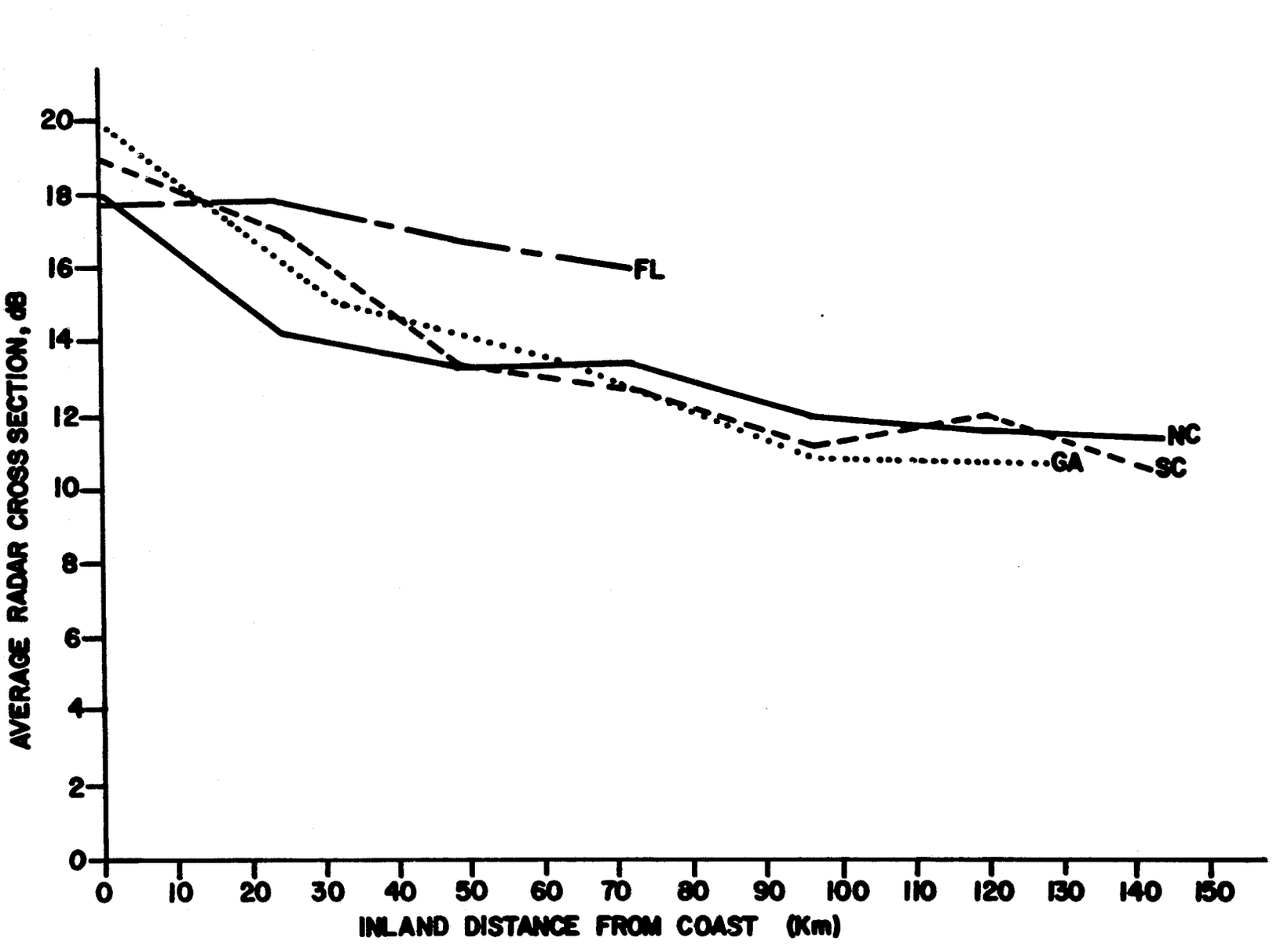

Figure 10. Variation of Radar Cross Section versus inland distance plotted on a common scale.

curves presented here have strict geographical regions of applicability, and if these constraints are not observed erroneous results will be incurred.

3.0 EFFECT OF ACTIVE FARMING OPERATIONS ON RADAR CROSS SECTION

The RCS of terrain is strongly dependent upon (1) soil moisture content, (2) surface roughness, and (3) a number of other parameters as discussed by Batlivala [3] and Ulaby et al. [4]. Measurements of radar cross section, and its dependence upon moisture and surface roughness, have been reported in these cited references. In order to separate the effects of moisture and roughness on RCS it was necessary to individually vary the two parameters and make the appropriate radar measurements. For GEOS-3 RCS measurements, controlled experiments such as those mentioned above are out of the question because of area coverage and lack of control of the subsatellite track. Therefore, any study of the effects upon RCS of active farming operations encounters the simultaneous variability of moisture content and surface roughness.

Because agricultural statistics were readily available, North Carolina was selected as the region for study in this phase of terrain data analysis. Roughly equal areas of land classed as farmland and nonfarmland were selected as shown by Figure 11. The counties resulting from this classification are listed in Table I. In order to be classed in the farmland category, it was required that 24% or more of the land in a given county be devoted to harvested cropland. The pertinent statistics for classification were obtained from [5] (it was assumed that the data in [5] for 1975 was also applicable to 1976 and 1977). The 21 counties included in the farmland category had an average of 32% harvested cropland while that of the 13 nonfarm counties was 10%.

A tabulation of GEOS-3 orbits used in compiling the data developed in this section is presented in Appendix 2. Curves of average RCS versus month of year for farmland and nonfarmland, developed from GEOS-3 passes over the

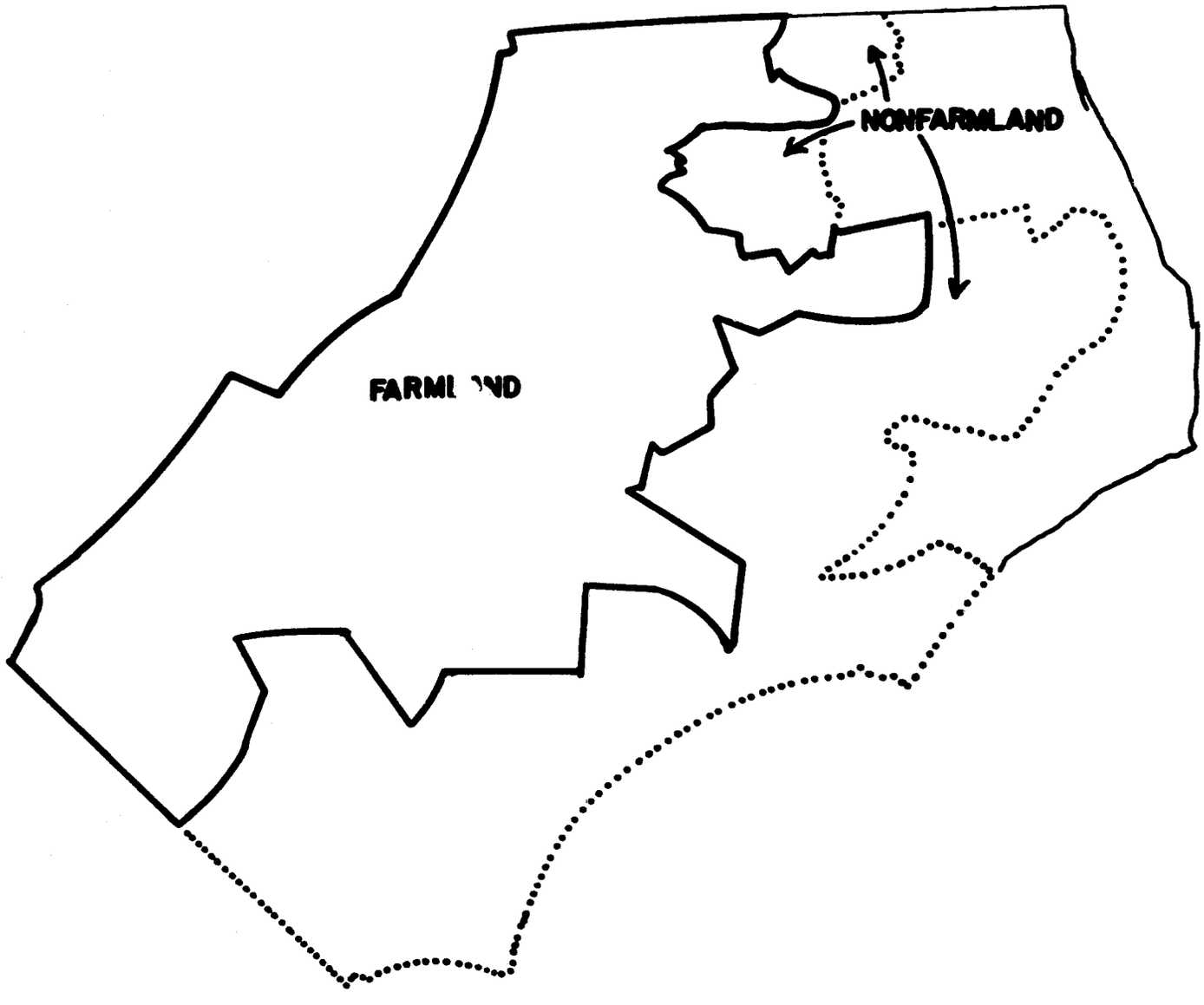

Figure 11. Classification of North Carolina terrain: farmland/nonfarmland.

TABLE I

County Classification of Region Used in Study

Farmland	Nonfarmland
Northamptor,	Gates
Hertford	Bertie
Halifax	Dave
Nash	Tyrrell
Edgecombe	Hyde
Martin	Beaufort
Washington	Craven
Wilson	Pamlico
Pitt	Carteret
Johnston	Onslow
Wayne	Pender
Greene	New Hanover
Pitt	Bladen
Lenoir	Brunswick
Jones	Columbus
Harnett	
Sampson	
Duplin	
Cumberland	
Hoke	
Scotland	
Robeson	

regions shown in Figure 11, are shown in Figure 12. A great deal of averaging of the altimeter RCS raw data was applied in drawing these curves which show a significant differential in RCS for the two terrain types over the months, 7, 8, 9, 10, 11, and 12. The average difference in RCS over this time period is about 3.4 dB while the maximum is approximately 4.5 dB. The maximum yearly change in RCS for farmland is about 8.5 dB for Figure 12.

An explanation of the above noted differences in RCS between farmland and nonfarmland leads to a subjective argument, but one which nevertheless agrees reasonably well with the available GEOS-3 data presented in Figure 12.* It is reasonable to assume that for the two types of terrain considered here, effects on RCS due to surface roughness are secondary to moisture effects [see 3]. Therefore, an explanation for the shape of the curves in Figure 12 will be sought in terms of soil moisture. Examination of climate-diagram maps [6] applicable to the region studied indicates potential evaporation effects can explain the observed variation of RCS. These same climate-diagrams [6] reveal that rainfall will also have a significant effect; however, it can be concluded that rainfall does not cause the observed variations since RCS should increase in response to rainfall. One is, therefore, led to suspect that potential evaporation (that is, the evaporating potential of the environment) is responsible for the effects observed on RCS. A disadvantage in using this parameter is that it is not widely recorded; however, within a climate type (e.g. humid), potential evaporation is related to temperature. Using data tabulated in [6] for Cape Hatteras, Wilmington, and Edenton (N. C.) the relative potential evaporation in dB for the region studied is plotted in Figure 13. This curve matches the observed effect rather closely in magnitude and time. It is noted that the RCS minimum for farmland lags that of

*Local soil moisture measurements would be required for verification. These data are unavailable.

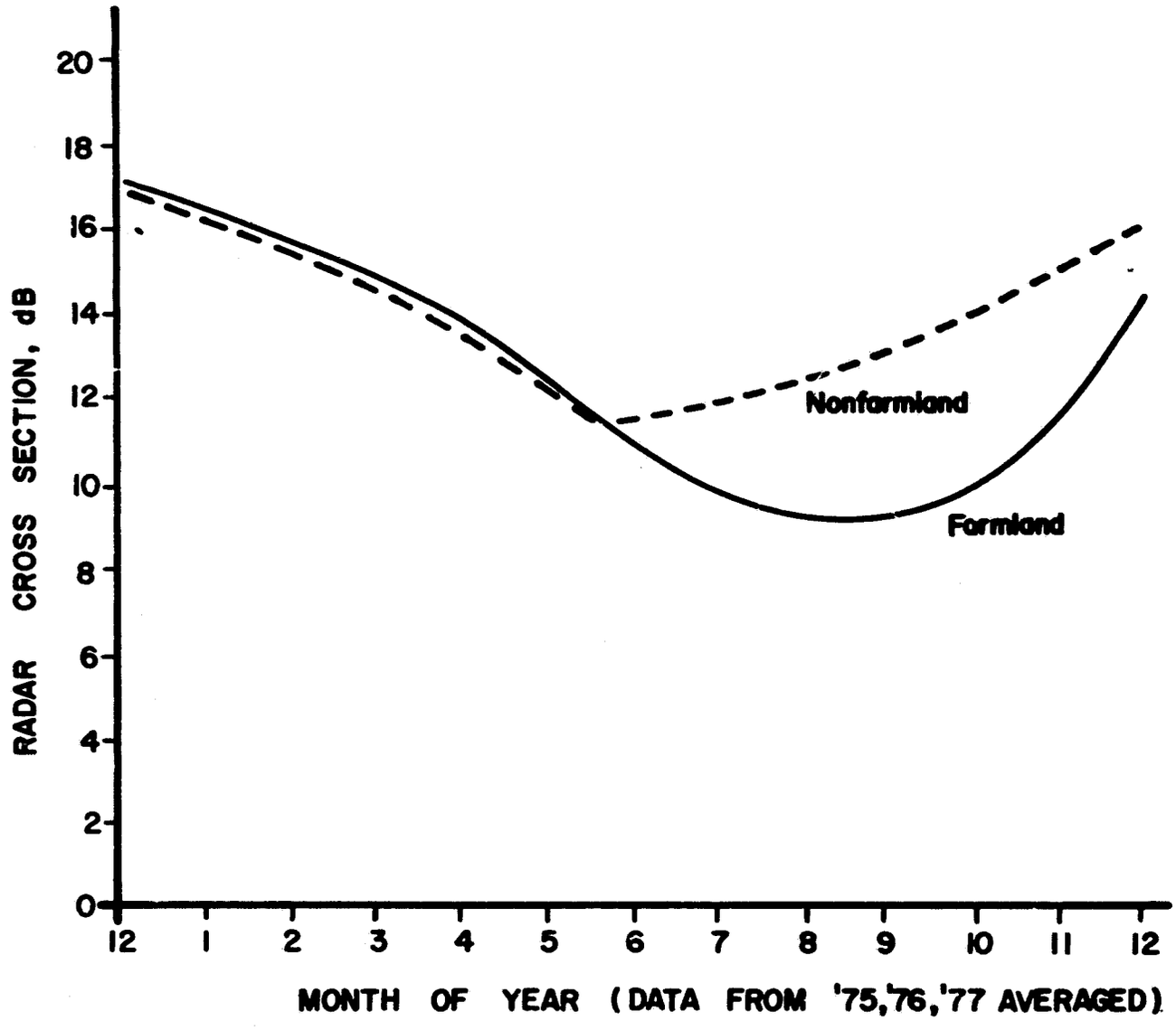

Figure 12. Variation of Radar Cross Section versus month of year for farmland and nonfarmland.

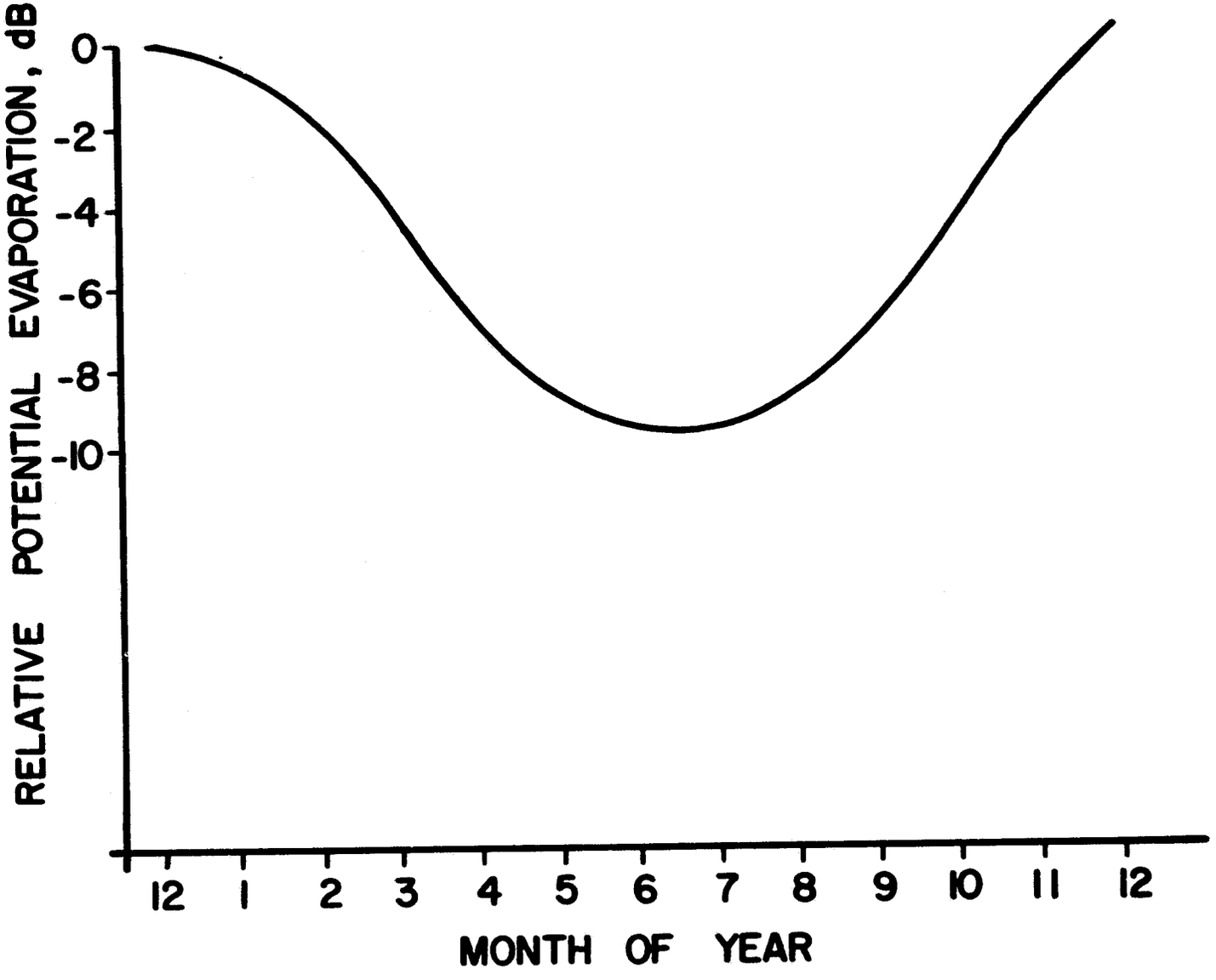

Figure 13. Potential relative evaporation versus month of year for Eastern North Carolina Region.

Figure 13 by about two months. It is also noted that nonfarmland terrain does not respond as strongly to the effects of the potential evaporation as does farmland and one would intuitively expect this result.

4.0 SEASONAL VARIATION OF RADAR CROSS SECTION

Plots of seasonal variation of RCS for North Carolina, South Carolina, Georgia, and Florida are shown in Figures 14 - 17 respectively. In compiling the data for these figures no distinction, other than state boundaries, was made. Therefore, effects of terrain variation and other classifications which might have been made are not presently considered.

The plot for North Carolina, Figure 14, is very interesting between months 6 to 12 as it falls about mid-way between the curves for nonfarmland and farmland of Figure 12 presented earlier. Examination of the curves for North Carolina, South Carolina, Georgia, and Florida (between the months of 2 - 11) indicate a general tendency of RCS to remain at a high value. That is, the effect of potential evaporation on RCS tends to decrease in progressing through the four states. This conclusion is to be expected since the effect of relative potential evaporation in South Florida [see 6] is very nearly constant (changing by only 0.5 dB during the year). The sudden drop in RCS for Florida during months 4 and 5 remains unexplained.

Dashed portions of these curves indicate less than three data points were available in drawing the Figures, while a missing segment (i.e. for Georgia) means no data point was available.

5.0 RADAR CROSS SECTION OF TERRAIN AND SOIL

In this section attention is directed to the tabulation of RCS for various terrain types and soil classifications. Resultant tabulations are based upon rather general and subjective classifications that are contained in [7]. The terrain classification data of [7] used in this section is presented in

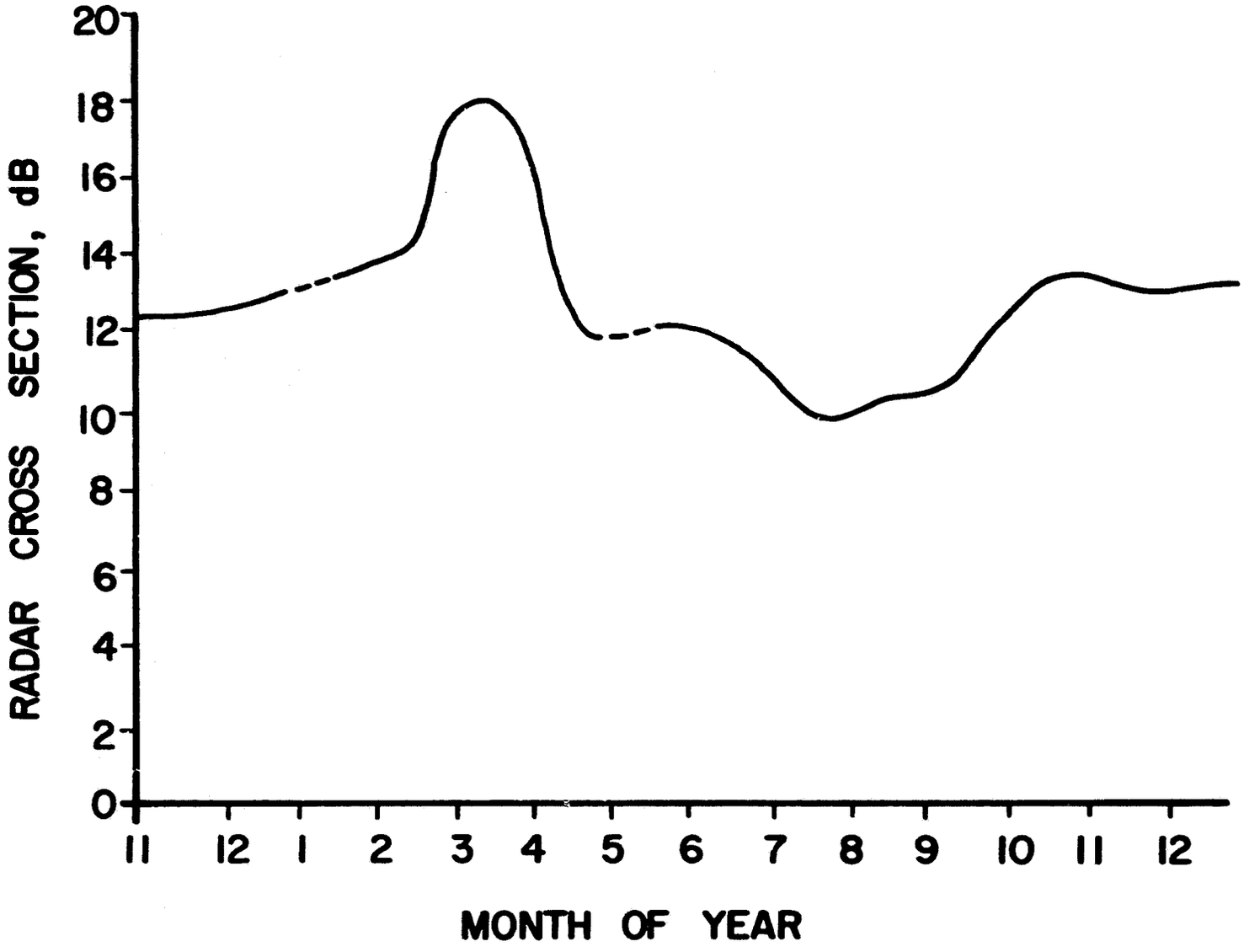

Figure 14. Radar Cross Section versus month of year for North Carolina.

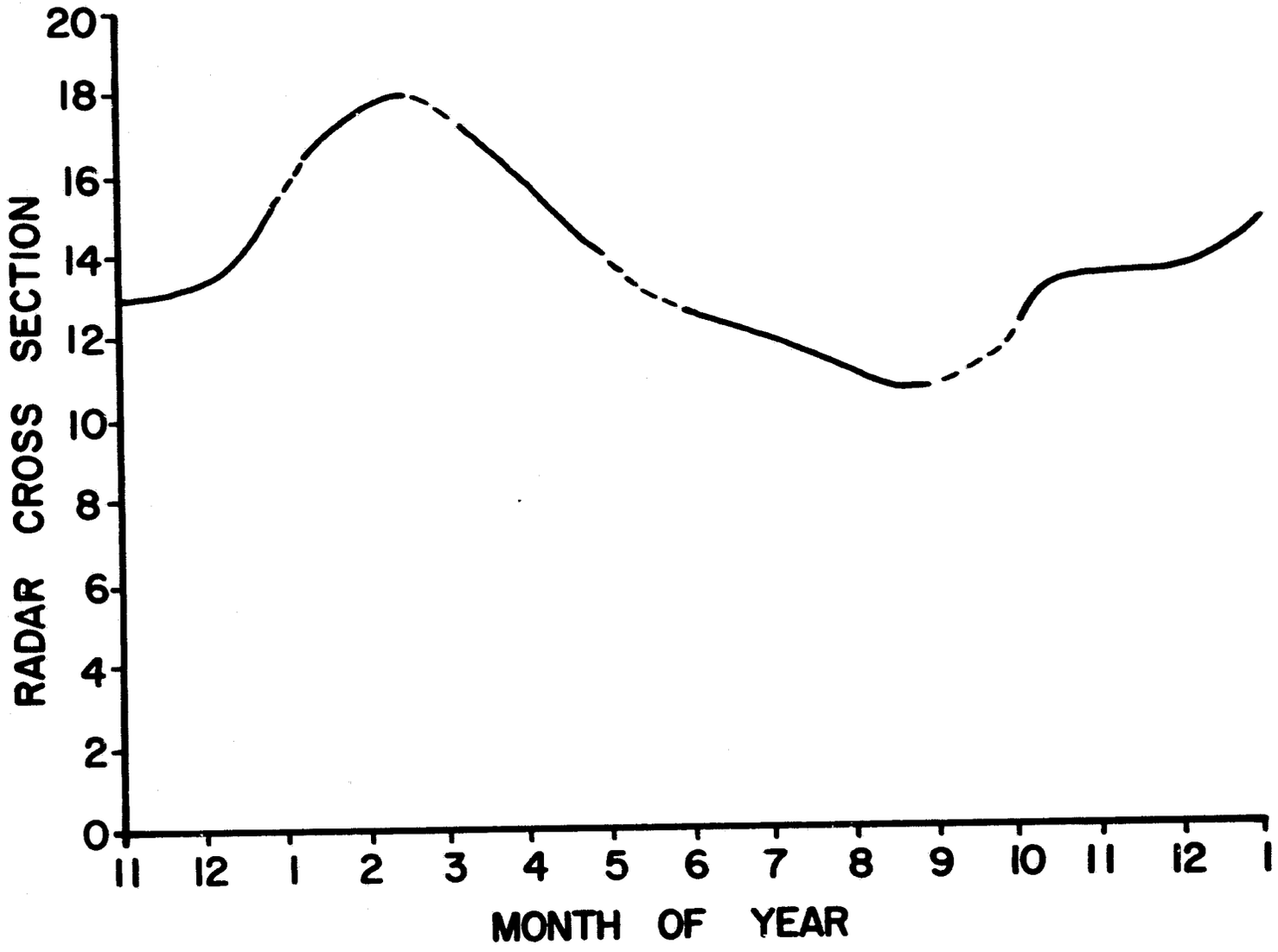

Figure 15. Radar Cross Section versus month of year for South Carolina.

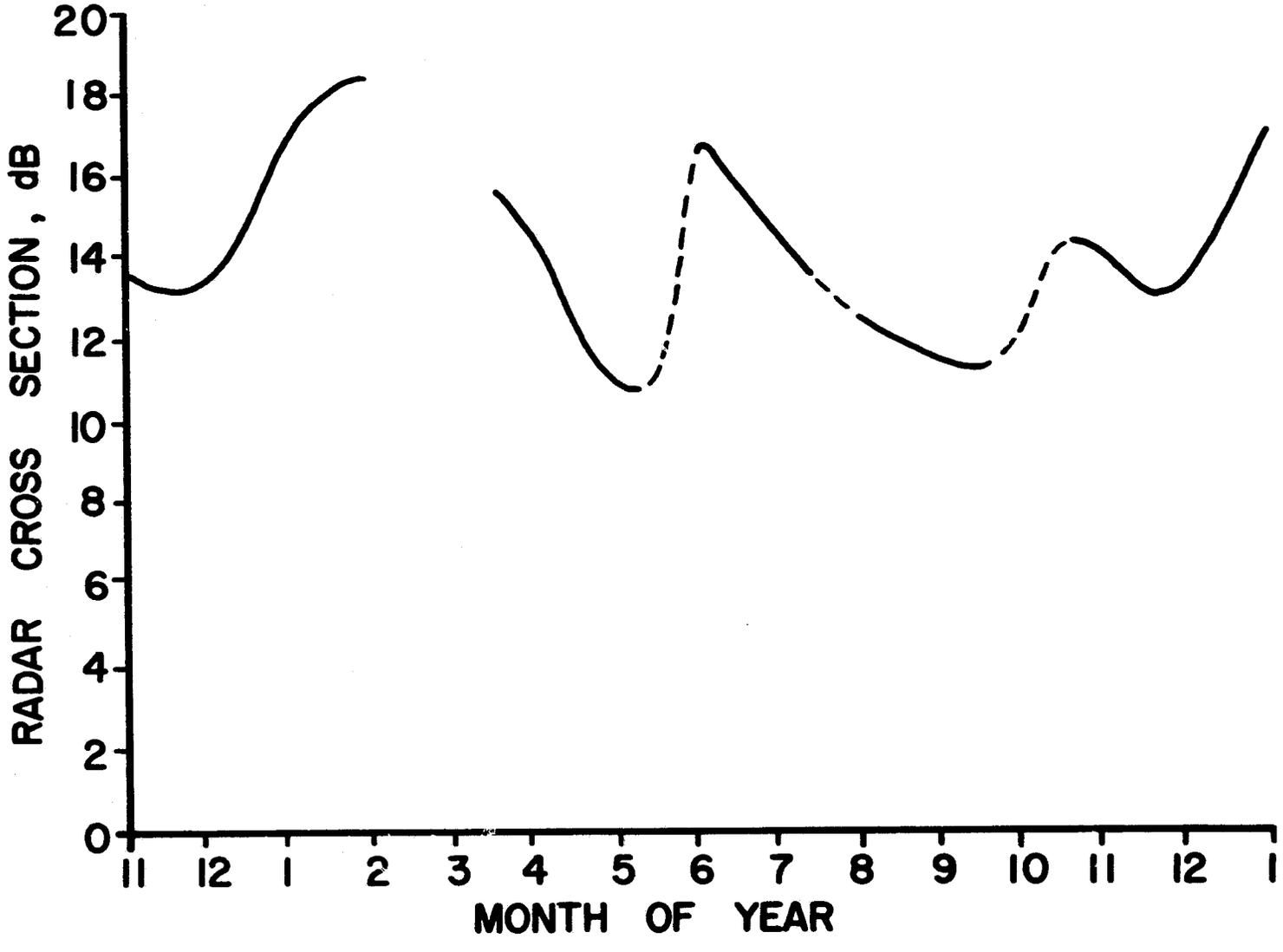

Figure 16. Radar Cross Section versus month of year for Georgia.

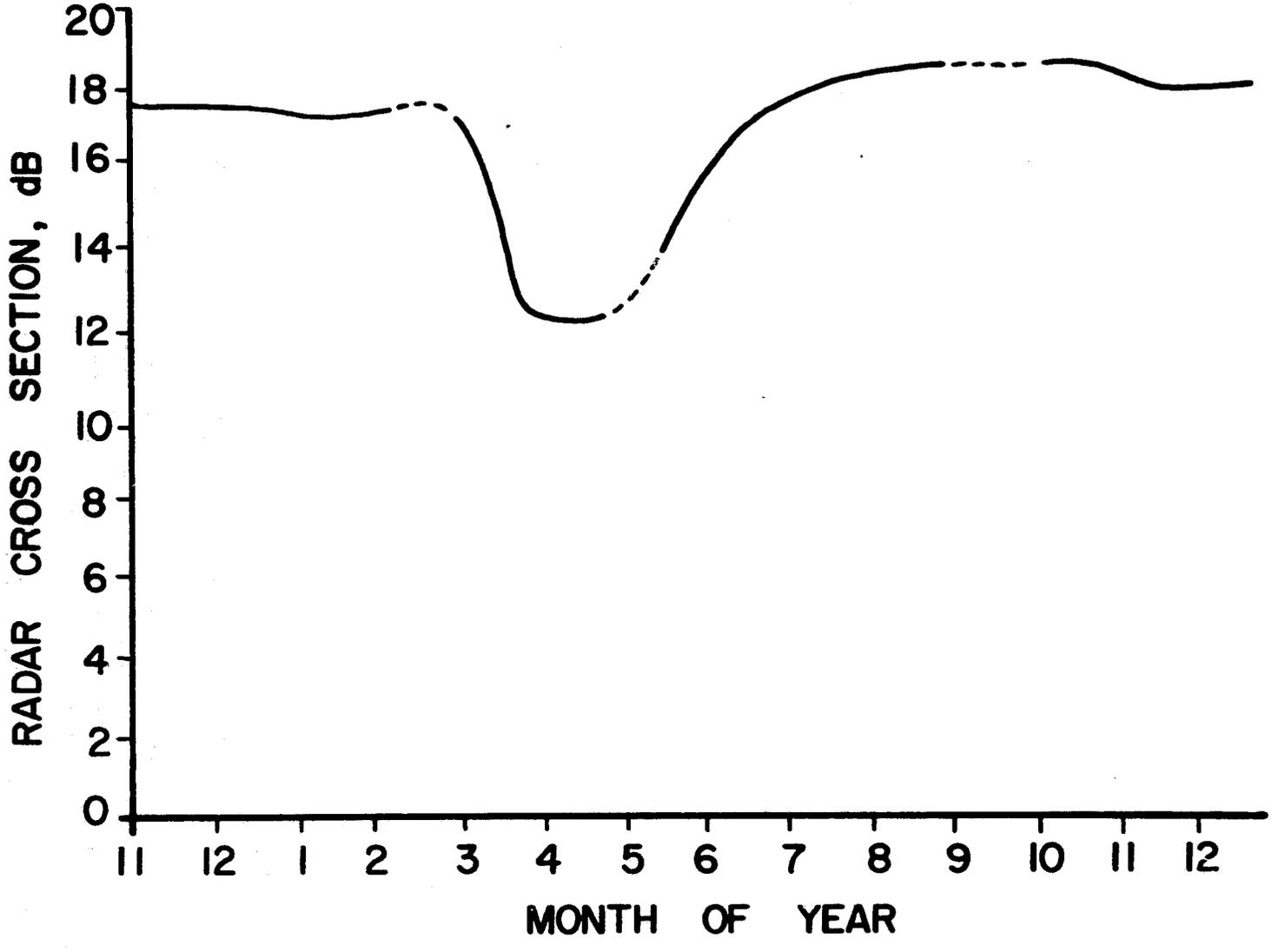

Figure 17. Radar Cross Section versus month of year for Florida.

Table II for convenience. Thus terrain classified as Alc would have the features (1) more than 80% of area gently sloping, (2) local relief varies from 0 to 91 m , and (3) more than 75% of gentle slope is in lowland. In like manner, the classification of soil types are rather general and subjectivity is deemed acceptable primarily for two reasons: (1) available soil classification maps invariably specify the presence of three or more dominant soil series (see [8], for example), and (2) the large swathwidth of the GEOS-3 footprint and averaging time required to compute reliable RCS value preclude fine detail. Thus, for the latter of these reasons detailed information on surface composition is not required for the present study.

TABLE II

Terrain Classification for Regions Studied

Slope Designation:

A: more than 80% of area is gently sloping
B: 50% to 80% of area is gently sloping

Local Relief Designation:

1: 0 to 30 m
2: 30 m to 91 m

Profile Type:

a: More than 75% of gentle slope is in lowland
b: 50% to 75% of gentle slope is in lowland
c: 50% to 75% of gentle slope is on upland

Average RCS was computed for selected regions that in some cases consisted of rather small area; the results are presented in Table III. These data show that very flat terrain with gentle slope and small relief has the largest RCS. This type of terrain typically is characterized by standing water (i.e. for the regions so classed in this work, usually more than 10% of the area is covered by standing water). It is noted that terrain classed as A1 and which is removed from the ocean interface has RCS ranging from about 13 to 16 dB (this class of terrain in Florida is characterized by a somewhat higher RCS, but this can be attributed to the fact that it is more than 50% covered by standing water). Apparently, this class of terrain exhibits a higher RCS, as compared with other types of terrain, due to its increased moisture and slightly undulating surface features.

For North Carolina farmland there is approximately a 2 dB difference in the yearly averaged RCS between farmland and nonfarmland. This compares with a maximum difference of about 4.2 dB on seasonal plots of average RCS as discussed in Section 3 of this report. Note that the terrain class of this comparison consisted of A1, A2c and B2c types and that the associated RCS is somewhat lower than that for A1 terrain.

Terrain covered by more than 50% sand has average RCS ranging from 7.3 dB to 11.3 dB. The relatively large value of 11.3 dB for Yuma, AZ., compared with lower values for Chicago and Fayetteville, NC., might result from the fact that relatively small data sets were used developing the Table 3 data for all of these regions.

Average RCS for upland terrain range from 5.8 dB to 11.5 dB. The resulting lower average for this drier and rougher terrain is to be expected.

TABLE III

RCS for Various Terrain Classifications

Terrain Description			RCS(dB)
Approximate Location	Comments	Classi-fication	
Chicago, IL	Marshlands near Lake Erie	A1	15.0
Coastal Plains, SC	Inland from ocean interface	A1	15.6
Coastal Plains, NC	Inland from ocean interface	A1	12.8
Coastal Plain, SC	At ocean interface	A1	19.3
Coastal Plain, NC	At ocean interface	A1	17.7
North Carolina	Active farmland	A1, A2c, B2c	12.2
North Carolina	Nonfarmland	A1, A2c, B2c	14.2
Yuma, AZ	At least 50% sand	A2b	11.3
Chicago, IL	At least 50% sand	A1	7.4
Fayetteville, NC	At least 50% sand	B2c	7.3
North Carolina		B2c	7.9
North Carolina		B2c	10.0
South Carolina		A2c	11.1
North Carolina		A2c	11.5
Lubbock, Texas		A2c	5.8

6.0 ANALYSIS OF AVERAGE RETURN WAVEFORMS OVER COASTAL PLAINS REGIONS

GEOS-3 average backscattered waveforms over terrain display a wide range of distinctive forms and some of these have been presented and discussed by Miller [1]. Both the surface backscattering properties and the tracker Automatic Gain Control (AGC) subsystem play an important role in the shaping of the terrain return waveform. In this section an approximate analytic expression is developed for the GEOS-3 return power waveform observed over coastal regions which are characterized by a very small scale of roughness superimposed on a gently undulating surface. This type of surface can give a variety of responses which apparently depend upon local surface features; however, a commonly observed waveform is one which displays a rather strong specular component in conjunction with a relatively weak diffuse return. This type surface response presents problems to the GEOS-3 split gate tracker which was designed for over-ocean operation. However, the GEOS-3 altimeter is able to track many of these waveforms in such a way as to provide useful topographic and other data (see [1]).

A common GEOS-3 waveform for coastal region operation can be characterized as having a very strong and rapid rise in amplitude during the early portion of the return (specular-like component) followed by an exponentially decreasing amplitude with increasing time. Since the AGC plateau gate is typically located in the exponential decay region of the response curve, saturation of some of the waveform samplers and/or video amplifiers frequently results from the strong specular component. Due to the fact that the ramp and plateau gates tend to "straddle" the saturated region of the average return waveform, tracker performance might not be affected in a drastic fashion (this remark ignores possible pulse stretching effects on the average return waveform caused by the saturating nonlinearity).

For over-ocean operation, the radar cross section can be considered, at a given locale, constant over the system antenna beamwidth. This situation is in contrast to that encountered over certain types of terrain for which earlier investigations [1], [9], have indicated that radar cross section varies according to the relation

$$\sigma^\circ(\psi) = \sigma^\circ(0)\ \exp[-\alpha \tan^2 \psi]$$

where ψ is the off nadir angle

α is a constant

$\sigma^\circ(0)$ is the radar cross section at nadir.

Given this model, Brown [10] has shown that the corresponding flat surface impulse function is given by

$$P_{FS}(\tau) \approx \frac{G_o^2\ \lambda\, c\, \sigma^\circ(0)}{4(4\pi)^2\ L_p h^3}\ \exp\left\{-\frac{4}{\gamma}\sin^2\xi - \frac{4c\tau}{h\gamma}\ \mathrm{Cos}^2\,\xi\right\}$$

$$\cdot\ I_o\left(\frac{4}{\gamma}\sqrt{\frac{c\tau}{h}}\ \mathrm{Sin}\ 2\xi\right)$$

$$\cdot\ \exp\left(-\frac{c\tau\,\alpha}{h}\right) \quad . \tag{1}$$

The factor $\exp(-c\tau\alpha/h)$ represents the effects of off nadir angle (via τ) on the measured backscattered waveform. Now, <u>assuming</u> that the surface small-scale roughness typical of coastal plains regions has a Gaussian probability density function

$$\frac{c}{2}\ q\left(\frac{c\tau}{2}\right) = \frac{1}{\sqrt{2\pi}\ \frac{2\sigma_s}{c}}\ \exp\left[-\frac{\tau^2}{2\left(\frac{2\sigma_s}{c}\right)^2}\right] \tag{2}$$

where c = speed of light expressed in m/n.-sec.

τ = delay time in n.-sec.

σ_s = surface roughness in meters ,

the rough surface scattering response function is given by the convolution of eq. (2) with eq. (1); therefore,

$$P_r(\tau) = \eta P_T \frac{G_o^2 \lambda c \sigma^\circ(0)}{4(4\pi)^2 L_p h^3} I_o\left(\frac{4}{\gamma}\sqrt{\frac{c\tau}{h}} \operatorname{Sin} 2\xi\right) \exp\left(-\frac{4}{\gamma}\operatorname{Sin}^2\xi - \frac{4c\tau}{\gamma h}\operatorname{Cos} 2\xi\right) \cdot$$

$$\cdot \frac{1}{\sqrt{2\pi\left(\frac{2\sigma_s}{c}\right)^2}} \int_{-\infty}^{\infty} \exp\left(-\frac{c\bar{\tau}\alpha}{h}\right) \exp\left[-\frac{(\tau-\bar{\tau})^2}{2\left(\frac{2\sigma_s}{c}\right)^2}\right] d\bar{\tau} \qquad (3)$$

where $P_r(\tau)$ is the expression for the measured average return power. It is possible to write (3) in the form shown because the factor $\exp(-c\tau\alpha/h)$ in (1) is the only term which varies significantly over the times τ of interest here. The integral expressed in (3) can be evaluated and is given by:

$$P_r(\tau) = \eta P_T \frac{G_o^2 \lambda c \sigma^\circ(0)}{4(4\pi)^2 L_p h^3} \frac{1}{\sqrt{2\left(\frac{2\sigma_s}{c}\right)^2}} I_o\left(\frac{4}{\gamma}\sqrt{\frac{c\tau'}{h}} \operatorname{Sin} 2\xi\right)$$

$$\cdot \exp\left(-\frac{4}{\gamma}\operatorname{Sin}^2\xi - \frac{4}{\gamma}\frac{c\tau'}{h}\operatorname{Cos} 2\xi\right) \cdot$$

$$\cdot \sqrt{\beta}\left\{\exp\left[\beta\Gamma^2 - \tau^2/\beta\right]\right\}\left[1 - \operatorname{erf}\left(\Gamma\sqrt{\beta}\right)\right] \qquad (4)$$

where $\Gamma = \frac{c\alpha}{h} - \frac{\tau}{2\beta}$

$$\beta = \frac{1}{2}\left(\frac{2\sigma_s}{c}\right)^2$$

$$\tau' = \begin{cases} 0 \ , & \tau < 0 \\ \tau \ , & \tau \geq 0 \end{cases}$$

η = pulse compression ratio

P_T = transmitter power .

Defining

$$y = \frac{2\beta\, c\,\alpha}{h} - \tau$$

$$P(\tau') = \frac{\eta\, P_T\, G_o^2\, \lambda\, c\, \sigma^\circ(0)}{4(4\pi)^2\, L_p h^3} \; \frac{\sqrt{\beta}}{\sqrt{2\left(\frac{2\sigma_s}{c}\right)^2}} \; I_o\left(\frac{4}{\gamma}\sqrt{\frac{c\tau'}{h}}\,\mathrm{Sin}\,2\xi\right) \cdot$$

$$\cdot \exp\left(-\frac{4}{\gamma}\,\mathrm{Sin}^2\xi - \frac{4}{\gamma}\,\frac{c\tau'}{h}\,\mathrm{Cos}\,2\xi\right)$$

eq. (4) can be written as follows:

$$P_r(\tau) = F(\tau')\left\{\exp\left[\frac{c\alpha}{h}\left(y - \beta\,\frac{c\alpha}{h}\right)\right]\right\}\left[1 - \mathrm{erf}\left(\frac{y}{2\sqrt{\beta}}\right)\right] \qquad (5)$$

For the case $\alpha = 0$, eq. (5) reduces to the form corresponding to constant $\sigma^\circ(\psi)$ [10] .

The preceding development has assumed a perfect altimeter instrument; however, the altimeter point target response effects on $P_r(\tau)$ can be accounted for by using a Gaussian functional form which is readily incorporated into the

above formulation. Thus by replacing $2\sigma_s/c$ in the above with $\sqrt{\sigma_p^2 + (2\sigma_s/c)^2}$, where σ_p is the point target effect in n.-sec., equation (5) can be used to model the scattering effects of some types of terrain.

This formulation has been used to fit GEOS-3 measured waveforms in coastal plains regions and appears to be capable of modeling waveforms for other types of terrain as well. However, random scattering of electromagnetic waves by terrain is a very complex problem involving combinations of point, specular, and random scattering processes. As a result equation (5) cannot be interpreted nor used as a general result. The sole, but appropriate, justification for its use here is that it adequately describes the data to which it has been applied in the development of results for this report.

In applying equation (5) to the problem of estimating σ_s and α, it appears that α is best estimated from the trailing portion of the return waveform. It is doubtful that the rising portion of the waveform contains sufficient sensitivity to both α and σ_s to enable their simultaneous estimation in this region. Once α is estimated as suggested above, σ_s can be obtained from the rising segment of the return.

A normalized plot of equation (5) with α, σ_s, and σ_p selected to fit an average GEOS-3 Intensive Mode waveform measured over coastal plain terrain is shown in Figure 18. The very rapid rise to peak followed by exponential decay often typifies backscatter for these regions. For the average waveform shown, the plateau gate of the split gate tracker is centered at about 52 n.-sec. Since the AGC loop maintains the plateau gate at approximately 100 mv the portion of the curve exceeding .73 would be saturated. Saturation of overland waveforms is common for the GEOS-3 tracker. It is clear from the figure why saturation occurs: AGC loop action is to set gain high enough to achieve 100 mv in the plateau gate which, due to t nential decay of the

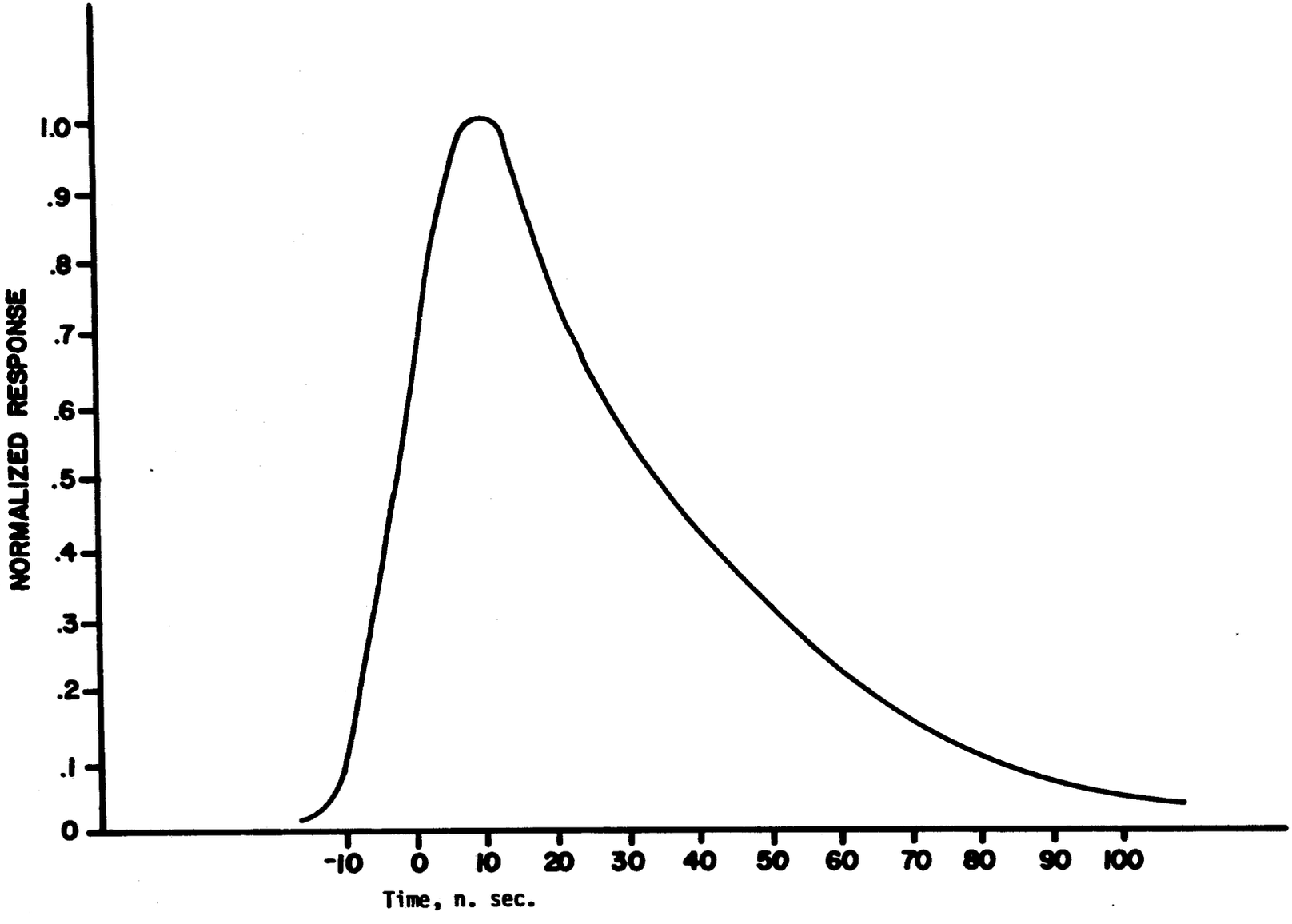

Figure 18. Normalized plot of equation (5).

waveform, can be a large value of gain. Thus the already strong portion of the early return is further amplified by the AGC action ultimately resulting in saturation.

The process described above can result in tracker bias due to the very rapid rise of the leading edge of the return waveform. Split-gate tracking interprets this as an earlier (in time) return which causes the surface to appear nearer to the altimeter. Ultimately the surface appears to be at a higher elevation with respect to sea level than would otherwise be the case. For the average waveform shown in Figure 18, this bias is 1.6 m as determined from a graphical analysis. It is emphasized that the bias effects discussed here are theoretical in nature; actual bias effects depend upon hardware implementation and operational characteristics.

For those situations where GEOS-3 overland data are of interest but suffer from saturation caused by AGC loop action, as described above, it is possible to approximately remove some of these effects. However only partial reconstruction of the waveform can be achieved and as a result its usefulness is limited. Based on the discussion of AGC loop action presented earlier it is known that for some types of terrain the gain applied by the system is excessive. Assume for the moment that the plateau gate of the AGC is positioned such that it measures the scale of the return waveform, V_{Pk}. Let the plateau gate measurement be denoted by $V_{P\ell}$. Now using the GEOS-3 sample-gate values $g_i (i=1,2,\ldots I)$ construct a new set of samples g_i' as follows

$$g_i' = \frac{1}{V_{P\ell}} \left(\frac{V_{Pk}}{V_{P\ell}} \right)^{-1} g_i \quad , \quad i=1,2,\ldots,I \tag{6}$$

where I is the index of the largest unsaturated gate. It can be seen that the g_i' are normalized to $V_{P\ell}$ and reduced by the factor $(V_{Pk}/V_{P\ell})^{-1}$.

Also note in equation (5) that for over-ocean tracking, $V_{P\ell} \simeq V_{Pk}$; therefore, in the case of over-ocean operation the g'_i are simply normalized versions of g_i . There are two obvious problems with the approach suggested: (1) it is difficult to estimate V_{Pk} , and (2) the integer I may be such that only a small portion of a return wave can be reconstructed. Often, however, it is possible to estimate V_{Pk} from unsaturated gate values of an average GEOS-3 return waveform. And, although graphical extrapolation may be required, it is possible to construct a modified average waveform by assuming symmetry about the 0.5 point on the normalized plot. This amounts to assuming a symmetric probability density function for the surface and that it has stationary statistics.

The method just described has been applied to a number of overland GEOS-3 average waveforms (coastal plains regions) and the resulting plots are presented in Figures 19-21. In these figures the measured waveforms (dashed curves) have been normalized to their measured peak value, $\max_i(g_i)$ so that they may be compared with the modified waveforms. The "early return" feature of the measured waveforms relative to the modified curves, as predicted above, is evident and plays a significant part in the resulting altitude bias. In addition, an analytic case has been analyzed with the result shown in Figure 22. The known peak of 1.4 was used in developing the data presented here and the results show good agreement with the case where $\sigma^\circ(\psi) = \sigma^\circ(0)$ (i.e. the solid curve). Using the preceding method, saturated GEOS-3 waveforms for coastal plains regions have been modified and used to estimate the rms surface roughness. Results show that rms surface roughness within the footprint varies from 0. m to 2.5 m in the few cases examined.

7.0 SUMMARY AND CONCLUSIONS

Maximum values of Radar Cross Section for the classes of terrain considered

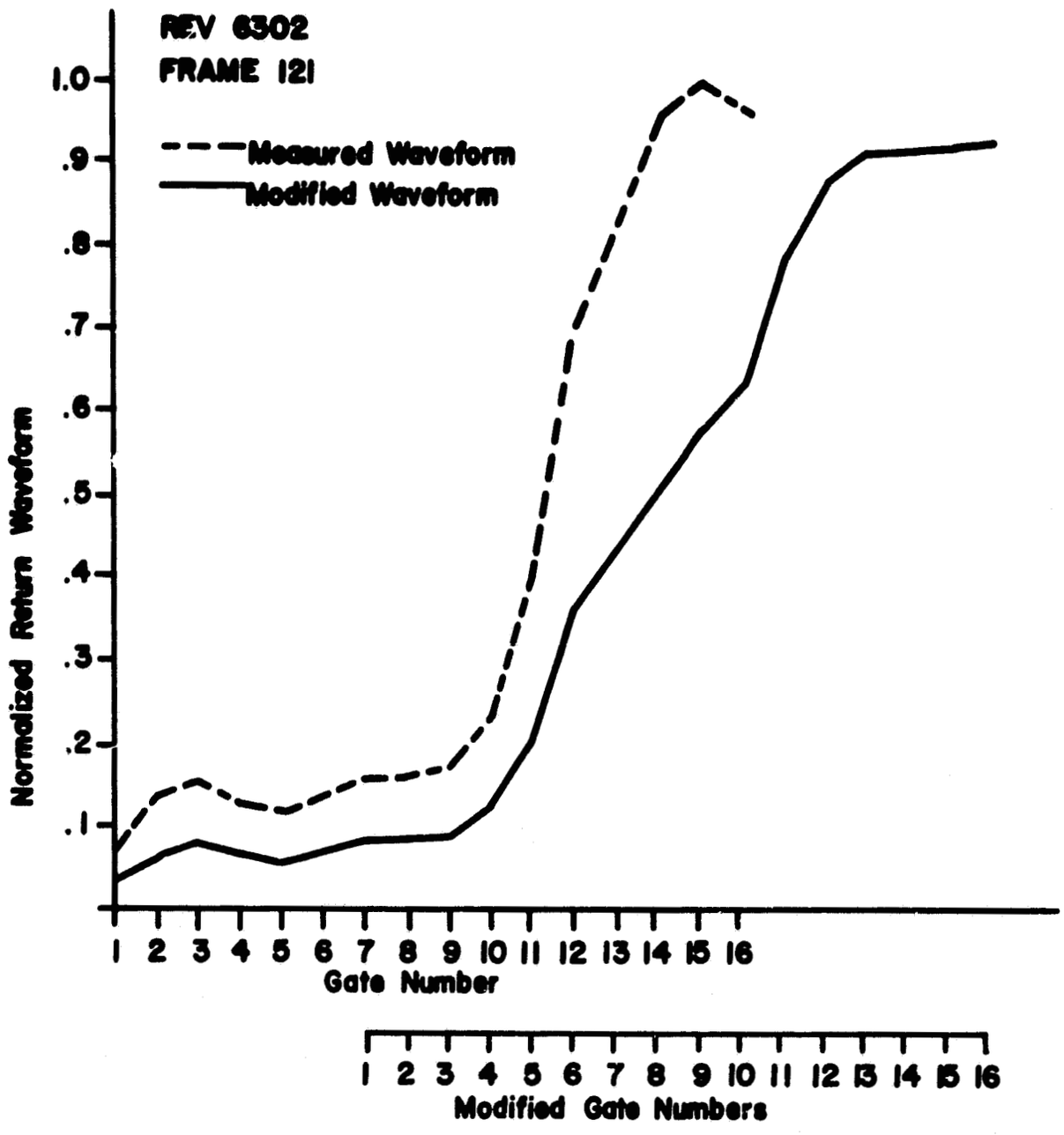

Figure 19. Modified GEOS-3 saturated waveforms measured over Coastal Plains terrain (modified gate numbers were used for computations of surface roughness).

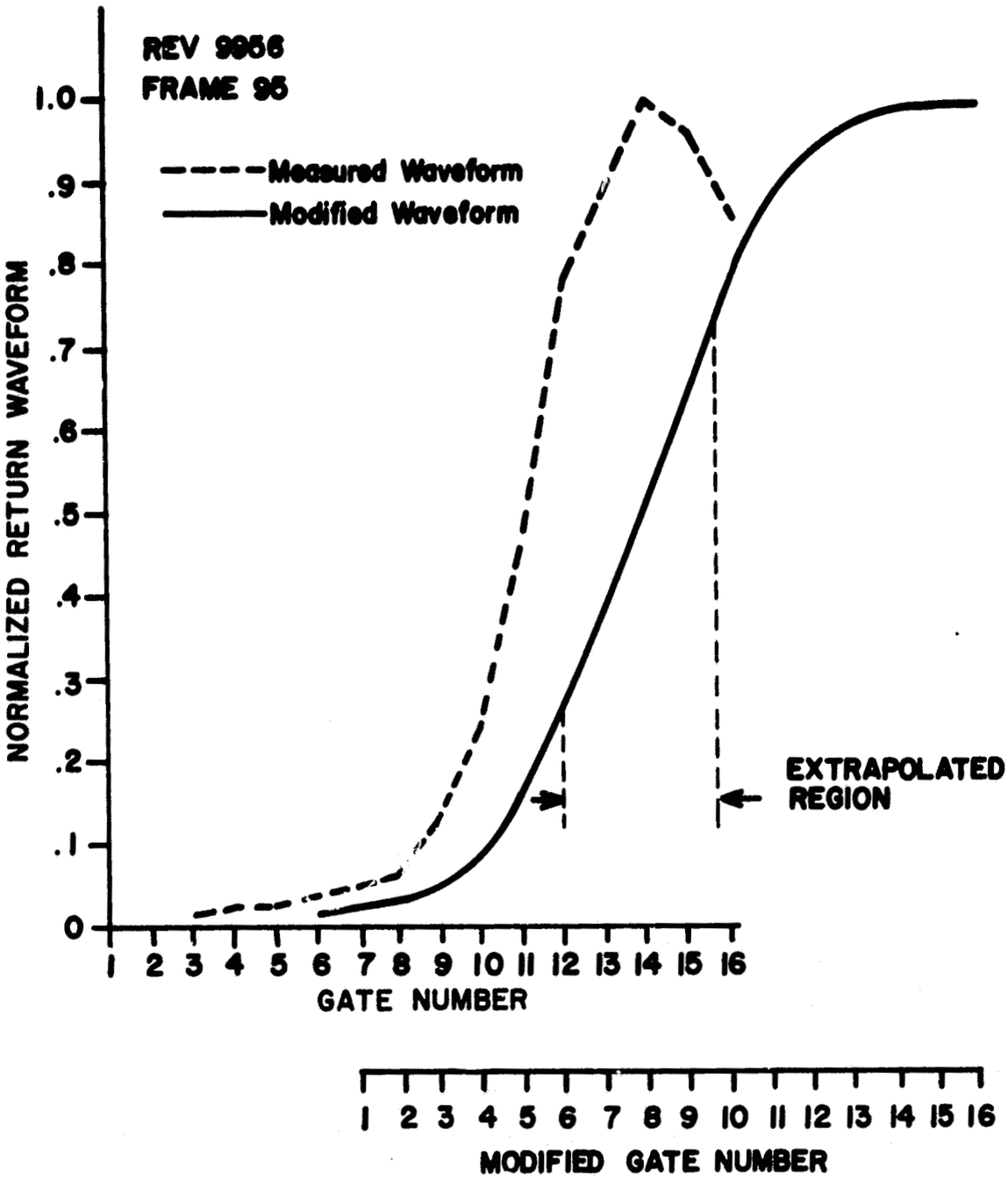

Figure 20. Modified GEOS-3 saturated waveforms measured over Coastal Plains terrain (modified gate numbers were used for computations of surface roughness).

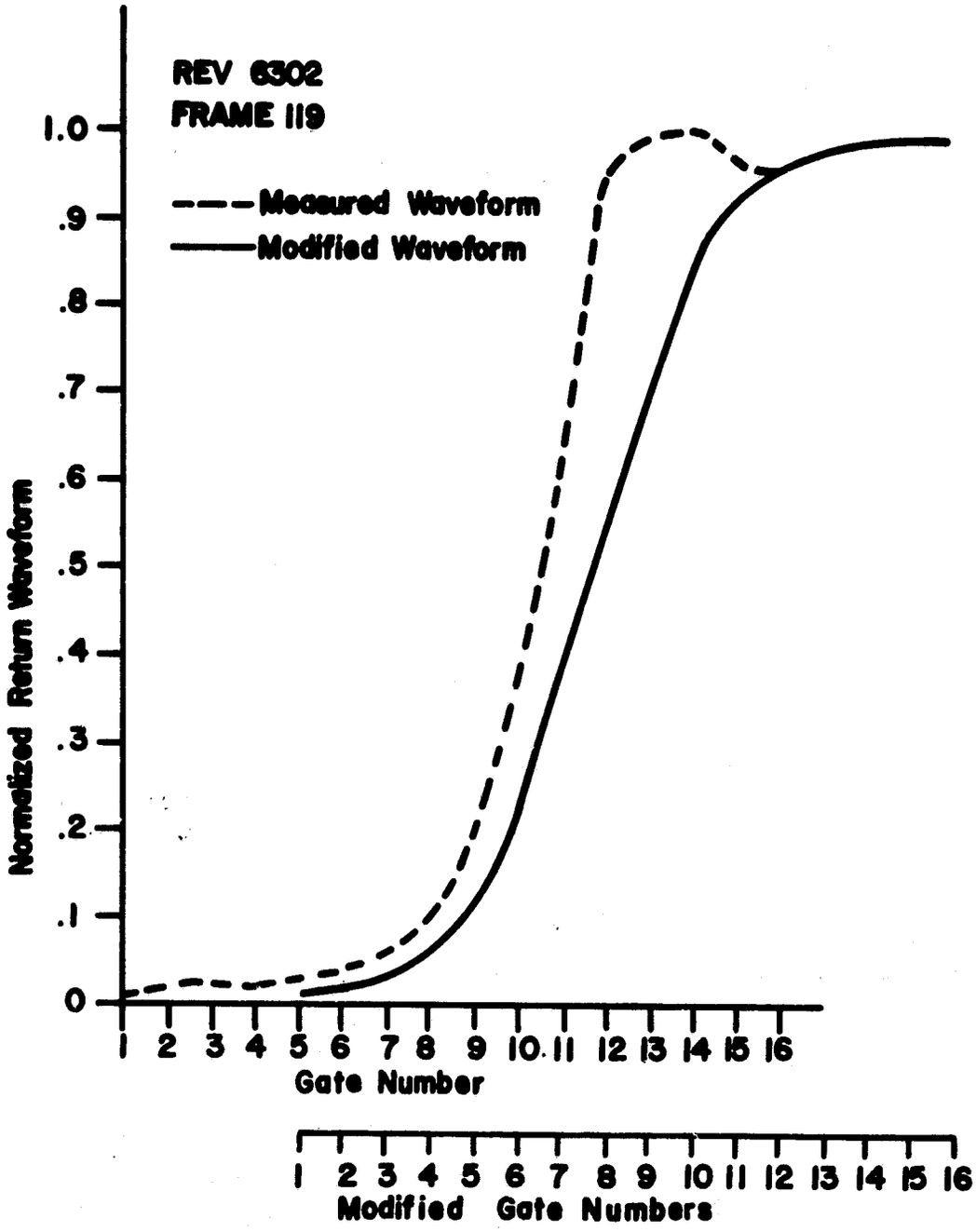

Figure 21. Modified GEOS-3 saturated waveforms measured over Coastal Plains terrain (modified gate numbers were used for computations of surface roughness).

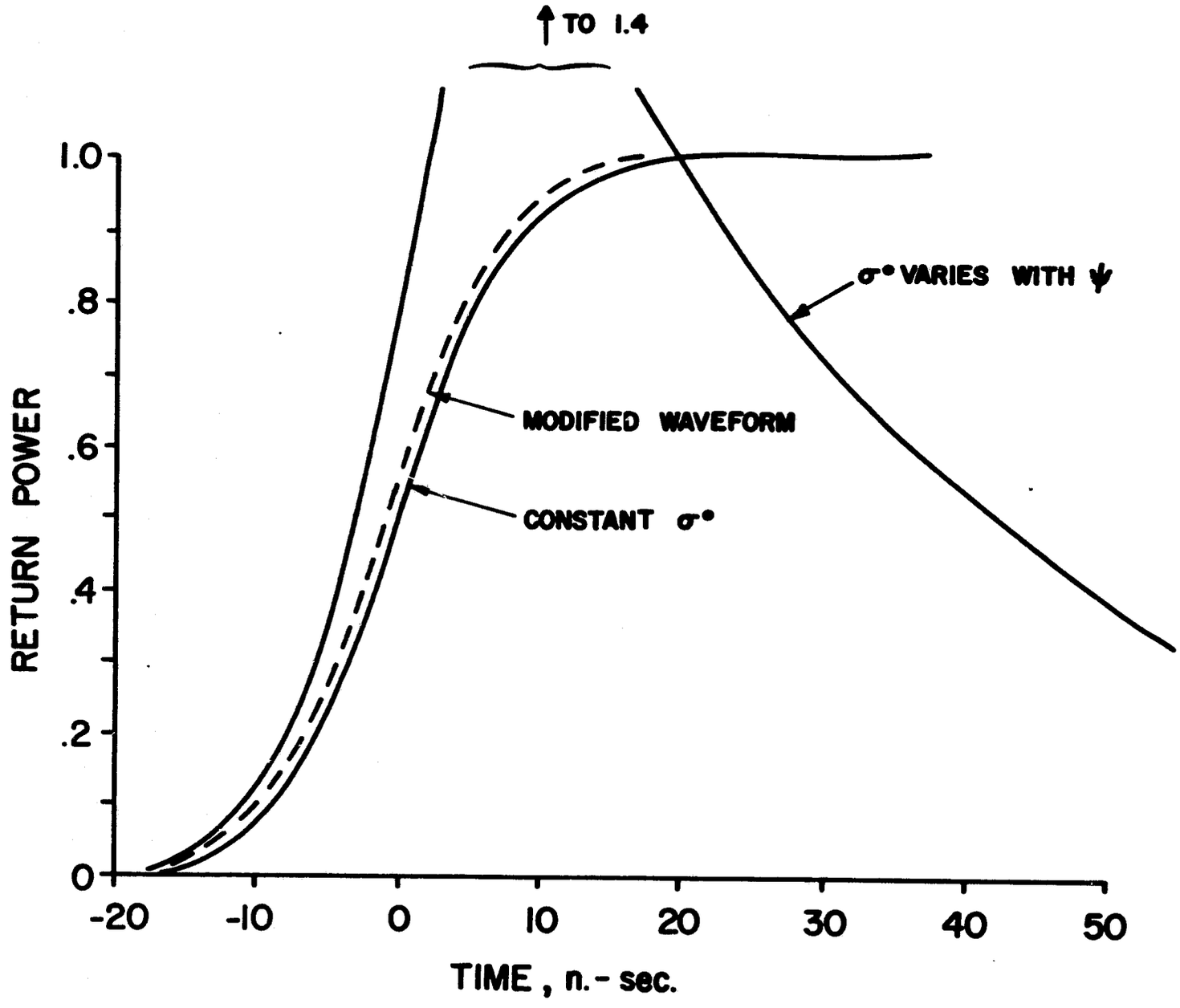

Figure 22. Modified analytic terrain waveform as computed from model of equation (5).

in this work occur at the land/ocean interface and in lowlands and/or swampy regions. Variation of RCS with inland distance from the coastline is approximately exponential typically starting at about 19 dB (average) and gradually decreasing to about 7 dB. Only average values of RCS have been discussed and for the data presented a one-sigma variation of about 4 dB is characteristic. Instantaneous fluctuations can be considerably larger ranging up to 10 dB in the data studied here (see also [1]).

A comparison of the RCS maps presented earlier with regional river systems maps, shows a direct correlation. Areas with high river system density also have higher RCS values while regions void of rivers reflect a lower RCS.

Farmland (i.e. harvested cropland) and nonfarmland appear to respond directly to the potential evaporation on a seasonal basis. Response of both types of terrain is very similar except that farmland is more responsive to potential evaporation in the growth and harvesting seasons. This suggests that the lower values of RCS observed for active farmland might result from a lower soil moisture content. That the potential evaporation function predominates in the seasonal variation of RCS is given additional credence by examining seasonal plots of RCS for the states of North Carolina, South Carolina, Georgia, and Florida. Of these four states, North Carolina has the largest variation in potential evaporation function while Florida has the smallest. This same variation is reflected into the seasonal changes of RCS.

In regard to GEOS-3 overland waveform analysis, an analytic development pertinent to backscattered waveforms frequently observed over coastal plains terrain was given and used to better understand tracking loop operation. It was found that the GEOS-3 tracker might not be greatly affected by the highly peaked waveforms encountered over some terrain types because saturation effects do not strongly impact the split-gate tracker. However, altitude bias errors

can result primarily from automatic gain control (AGC) subsystem effects. The analytic model presented is of limited utility in the general terrain scattering problem since it attempts to model a very complex situation via a single function: $\sigma^{\circ}(\psi)$. While this approximation agrees with observation in many situations, it cannot be indiscriminately applied.

A graphical method was presented and corroborated for recovering terrain surface roughness data from the early portion of saturated GEOS-3 waveforms via an analytic example. The technique has been devised to overcome effects of the tracker AGC subsystem which can distort the return waveform measured over terrain.

RCS data for very rough, mountainous terrain was not included in this study. Such an analysis probably should be performed by automatic means due to an increased need for data editing. It readily follows that RCS maps of any area of interest might be drawn by automatic means provided that sufficient coverage density exists in the GEOS-3 data base.

8.0 ACKNOWLEDGEMENTS

G. S. Hayne, N. Roy, and the GEOS-3 Eclipse data center staff at Wallops Flight Center provided much assistance in obtaining the data used in this study. The cooperation of Carl Gary (Weyerhauser, Inc.), Bob Richardson (Federal Paperboard), and F. W. Smith (International Paper Company) is gratefully acknowledged. Data supplied by these gentlemen was to be used in an attempt to detect timber harvesting operations. It was impossible to conclude this phase of the investigation because of the smallness of harvested areas relative to the GEOS-3 footprint.

REFERENCES

[1] Miller, L. S.: Investigation of the Application of GEOS-3 Radar Altimeter Data in Remote Sensing of Land and Sea Features, NASA Contractor Report, NASA CR-141428, Wallops Flight Center, Wallops Island, VA., August, 1977.

[2] Brown, G. S. and Curry, W. J.: The Estimation of Pointing Angle and σ° from GEOS-3 Radar Altimeter Measurements, NASA Contractor Report, NASA CR-141426, Wallops Flight Center, Wallops Island, VA., August, 1977.

[3] Batlivala, P. P., On the Feasibility of Monitoring Soil Moisture Using Active Microwave Remote Sensing: An Experimental Evaluation, Ph.D. Thesis, Department of Electrical Engineering, University of Kansas, 1971. Available from University Microfilms International.

[4] Ulaby, F. T. et al.: Microwave Backscatter Dependence on Surface Roughness, Soil Moisture, and Soil Texture: Part I - Bare Soil, IEEE Transaction on Geoscience Electronics, Vol. GE-16, No. 4, pp. 286-295, October, 1978.

[5] North Carolina Agricultural Statistics - 1977, Prepared by North Carolina Crop and Livestock Reporting Service, 1 West Edenton St., Raleigh, NC.

[6] Walter, H., Harnickell, E., and Mueller-Dombois, D.: Climate-diagram Maps, Springer Verlag, New York, 1970.

[7] Classes of Land-Surface Form, Adapted from Edwin H. Hammond, "Classes of land surface form in the forty-eight-States, U.S.A.," Annals of the Association of American Geographers, Vol. 54, No. 1, 1964 (map supplement No. 4, scale 1:5,000,000).

[8] Santee River Basin Water and Land Resources; Prepared by United States Department of Agriculture; Economic Research Service, Forest Service, and Soil Conservation Service, September, 1973.

REFERENCES (Cont'd.)

[9] Miller, L. S., Brown, G. S., and Priester, R. W.; A Summary of GEOS-3 Data Studies, Applied Science Associates, Inc., Internal Technical Report, November, 1977.

[10] Brown, G. S., The Average Impulse Response of a Rough Surface and its Applications, IEEE Transactions on Antennas and Propagation, Vol. AP-25(1), pp. 67-74, January, 1977.

APPENDIX 1

GEOS-3 Orbits Used in Constructing Radar Cross Section Maps and Related Material

Orbit Number	Date of Orbit	Orbit Number	Date of Orbit
2017	750830	10433	770416
2543	751006	6552	760716
3794	760103	3069	751112
1164	750701	4846	760317
6424	760707	5898	760530
1889	750821	6950	760813
1363	750715	2941	751103
837	750608	3140	751117
6623	760721	7149	760827
1562	750729	5244	760414
3666	751225	3339	751202
2287	750918	7078	760822
3865	760108	5372	760423
2464	751001	3993	760117
9103	770112	6097	760613
11861	770726	5770	760521
6772	760724	7860	761016
11335	770619	5955	760603
9956	770313	11670	770712
12188	770818	10291	770406
10809	770512	9438	770205
11662	770712	6154	760617
3516	751214	3197	751121
10283	770405	246	750427
6473	760710	2876	751030
6800	760802	3402	751206
2791	751024	3729	751229
10084	770322	2677	751016
11264	770614	3203	751122
3189	751121	6160	760618
3516	751214	9970	770314
4568	760226	2478	751002
10234	770402	3004	751108
8855	761225	10297	770406
9387	770201	7866	761016
9054	770108	3331	751201
11613	770708	6814	760803

APPENDIX 1 (Cont'd.)

Orbit Number	Date of Orbit	Orbit Number	Date of Orbit
10098	770323	12196	770819
2606	751011	6154	760617
3132	751117	9964	770314
6089	760613	6680	760725
2933	751103	10490	770420
4596	760228	3197	751121
10311	770407	5301	760418
3018	751109	5827	760525
2492	751003	10163	770328
6501	760712	6879	760808
12017	770806	2344	750922
3345	751202	2870	751029
2819	751026	4448	760218
10112	770324	11818	770723
12344	770829	10439	770416
6302	760628	10240	770402
5776	760522	11946	770801
6629	760721	12273	770824
3146	751118	11747	770718
2620	751012	12202	770819
11292	770616	9444	770205
9913	770310	11676	770713
3473	751211	12003	770805
2947	751104	9245	770122
6956	760813	6288	760627
6430	760707	11477	770629
1170	750701	12330	770828
9188	770118	11804	770722
4852	760317	10425	770415
2748	751021	12135	770814
7283	760905	11605	770708
6752	760730	6942	760812
6231	760623	8847	761225
7084	760822	6615	760720
2549	751007	3459	751210
3075	751113		
11221	770611		

APPENDIX 2

A. Farmland

Orbit Number	Date of Orbit	Orbit Number	Date of Orbit
11221	770611	7860	761016
3075	751113	5955	770603
2549	751007	10291	770406
7084	760822	11670	770712
6231	760623	9438	770205
6757	760730	12196	770819
7283	760905	6154	760617
2748	751021	9964	770314
4852	760317	6680	760725
9188	770118	10490	770420
1170	750701	3197	751121
6430	760707	5301	760418
6956	760813	5827	760525
3473	751211	11747	770718
2947	751104	12273	770824
3473	751211	11946	770801
9387	770201	10240	770402
9913	770310	10439	770416
11292	770616	11818	770723
9060	770109		
2620	751012		
3146	751118		
6629	760721		
5776	760522		
6302	760628		
12344	770829		
10112	770324		
2819	751076		
3345	751202		
12017	770806		
6501	760712		
2492	751003		
3018	751109		
10311	770407		
4596	760228		

B. Nonfarmland

Orbit Number	Date of Orbit
11221	770611
246	750427
3075	751113
2549	751007
7084	760822
6231	760623
6757	760730
7283	760905
2748	751021
4852	760317
9188	770118
1170	750701
6430	760707
6956	760813
2947	751104
3473	751211
9387	770201
9913	770310
11292	770616
3146	751118
6629	760721
5776	760522
6302	760628
12344	770829
10112	770324
2819	751026
3345	751202
12017	770806
6501	760712
2492	751003
3018	751109
10311	770407
9438	770205
12196	770819
6154	760617
9964	770314
6680	760725
3197	751121
5301	760418
5827	760525
10163	770328
6879	760808
2344	750922
2870	751029
4448	760218
11747	770718
12273	770824
11946	770801

1. Report No.	2. Government Accession No.	3. Recipient's Catalog No.
NASA CR-156865		

4. Title and Subtitle	5. Report Date
A STUDY OF GEOS-3 TERRAIN DATA WITH EMPHASIS ON RADAR CROSS SECTION	September, 1979
	6. Performing Organization Code
7. Author(s)	8. Performing Organization Report No.
R. W. Priester	
	10. Work Unit No.
9. Performing Organization Name and Address	11. Contract or Grant No.
Applied Science Associates, Inc. 105 East Chatham Street Apex, N. C. 27502	NAS6-2810
	13. Type of Report and Period Covered
12. Sponsoring Agency Name and Address	Final Report
National Aeronautics and Space Administration Wallops Flight Center Wallops Island, Virginia 23337	14. Sponsoring Agency Code

15. Supplementary Notes

16. Abstract

Radar cross section (RCS) of terrain is studied using GEOS-3 radar altimeter data. Maps of RCS for portions of four east coast states (U.S.A.) are presented and used to draw curves of RCS versus inland distance as measured from the land/sea interface. The results show RCS to decay approximately exponentially with inland distance. GEOS-3 data is also used to develop curves of RCS seasonal variation for the same regions. Observed variations correlate strongly with local potential evaporation. Results of the study also show that farming operations in the state of North Carolina are observable in the RCS data. A restricted method for determining surface roughness features from saturated average return waveforms for some types of terrain is developed. Sensor bias induced by receiver saturation for certain terrain returns is briefly discussed.

17. Key Words (Suggested by Author(s))	18. Distribution Statement
Radar Cross Section Overland Backscatter Remote sensing	Unclassified - unlimited STAR Category - 42, 43, 46

19. Security Classif. (of this report)	20. Security Classif. (of this page)	21. No. of Pages	22. Price*
Unclassified	Unclassified	49	

*For sale by the National Technical Information Service, Springfield, Virginia 22151